CrossMark

ORIGINAL ARTICLE

# Geothermometry and circulation depth of groundwater in Semnan thermal springs, Northern Iran

Soraya Karimi[1] · Zargham Mohammadi[1] · Nozar Samani[1]

**Abstract** Semnan thermal springs with high TDS and moderate temperature are located northwest of Semnan, the northern part of Iran. The spatial and temporal variations of physicochemical characteristics of the thermal and cold springs were investigated for the recognition of origin and dominant hydrogeochemical processes. Results show that the thermal springs have the same origin, but due to different ascending flow paths and different conductive cooling mechanism, their temperatures vary. The chemical composition of thermal waters is controlled by dolomite, halite and sulfate minerals dissolution and calcite precipitation and bacterial sulfate reduction. The concentration of major and trace elements in the thermal springs does not change in wet and dry seasons notably because they are derived from old groundwater with deep circulation and high temperature. Seasonal change in the concentration of some trace elements is due to the seasonal variation of pH, Eh, temperature and dilution by shallow waters. Decreasing $SO_4$ and carbonate saturation index and increasing Na/Cl ratios and Ca content in the dry season show dilution effect caused by the previous heavy rainfall events. The temperature of the heating reservoir based on K–Mg, chalcedony, quartz and chemical equilibrium approach was approximately estimated in the range of 60–80 °C. Hydrogeologically, a conceptual model was suggested for the thermal springs. The general groundwater flow direction is probably from the dolomite Lar Formation in Chenaran anticline toward the adjacent syncline in a confined condition, and then a thrust fault acts as a conduit and

redirects the thermal water to the emerging springs at the surface.

**Keywords** Geothermometry · Hydrogeology · Thermal spring · Semnan · Iran

## Introduction

Geothermal energy is developed for power generation and heat production because it is environmentally cleaner than fossil fuels. Thermal springs are one of the surface indications for the geothermal energy resources. In order to characterize thermal springs, their hydrogeochemistry and hydrogeology have been investigated. Studies on thermal springs commonly use chemical, physical and isotopic characteristics of water to delineate the origin of geothermal water (Ma et al. 2009; Pasvanoğlu and Chandrasekharam 2011; Lambrakis and Kallergis 2005), the mixing mechanism of geothermal fluid (Pürschel et al. 2013; Han et al. 2010; Asta et al. 2012; Majumdar et al. 2009; Ben Brahim et al. 2014), water–rock interaction processes (Farr and Bottrell 2013; Alçiçek et al. 2016; Han et al. 2010; Gunn et al. 2006; Asta et al. 2012), water circulation conceptual models (Farr and Bottrell 2013; Han et al. 2010; Marques et al. 2013; Alçiçek et al. 2016), the age of thermal waters (Farr and Bottrell 2013) and the reservoir temperature (Asta et al. 2012; Tarcan and Gemici 2003; Chulli et al. 2012; Chandrajith et al. 2013; Majumdar et al. 2009).

Iran's plateau provides some 400 geothermal resources with low to moderate temperature (Ghafori 1987). Geologically, Iran is divided into five major geological units (Fig. 1), including (1) Zagros, (2) Central Iran, (3) Sanandaj-Sirjan, (4) East and South East zones and (5) Alborz (Stöcklin 1968; Alavi 2004). The last unit, Alborz,

✉ Zargham Mohammadi
zmohammadi@shirazu.ac.ir

1   Department of Earth Sciences, Shiraz University,
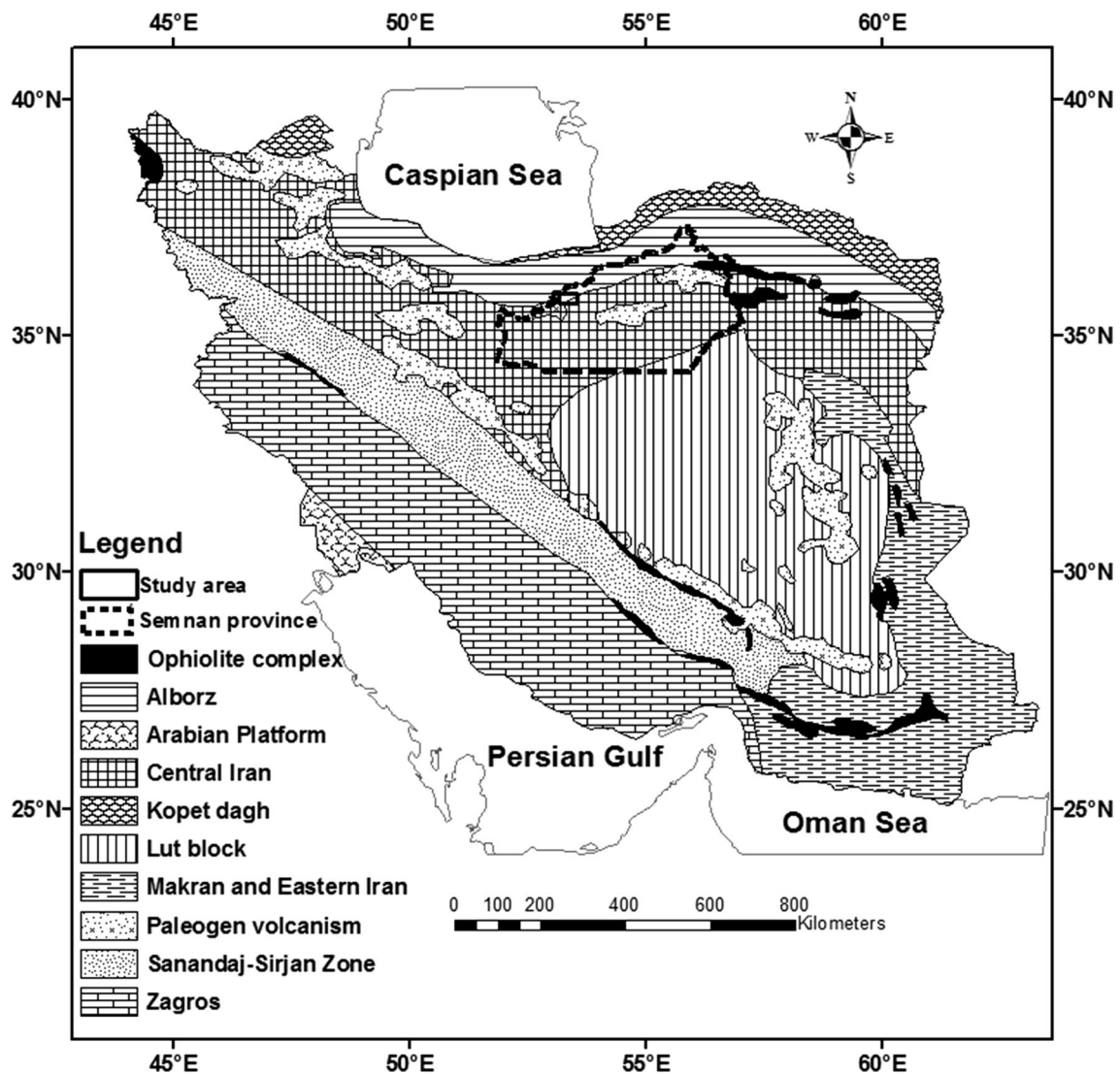    Shiraz 71454, Iran

**Fig. 1** Sedimentary and structural zones of Iran and the location of study area (modified from Stöcklin 1968)

has many thermal springs and geothermal resources due to the most active recent volcanism (Noorollahi et al. 2009).

The most studies in Iran have focused on the nature, reservoir temperature and chemical evolution of Zagros thermal springs. For example, Kompani-Zare and Moore (2001) reported that the source of Dalaki thermal spring is mixed meteoric water and oilfield brine and its high temperature is due to exothermic reaction and the deep circulation of water through the faulted system. Mohammadi et al. (2010) used different geothermometers and mineral saturation indices and estimated the source temperature of the Changal thermal springs emerging from Asmari limestone to be between 70 and 80 °C. Karimi and Moore (2008) studied the source and heating mechanism of Ahram, Mirahmad and Garu thermal springs with the average temperature of 40 °C. Based on the isotopic and chemical analyses, they concluded that the deep circulation

of meteoric water and contact with Hormoz Series evaporites, and the oilfield brines promoted the dissolved ion concentrations. Also, some researches have been conducted in Central Iran zone (Mohammadi and Parizi 2013; Yazdi et al. 2015; Sharifi et al. 2016). The heating mechanism of the studied thermal springs was similar to the studies mentioned in the Zagros region. Usually, the extended water–rock interaction and contact with evaporite formations and mixing with brines have controlled their chemistry (Fig. 2).

A few studies have been conducted in the chemical characteristics and geothermometry of thermal springs with low to moderate temperature in Alborz zone (Shamsi and Kazemi 2014). Raghimi and Yakhkashi (2002) examined the origin of the Ziarat thermal spring based on the isotope and hydrochemical methods and compared it with some springs in Alborz of similar water type (Na–Cl) and
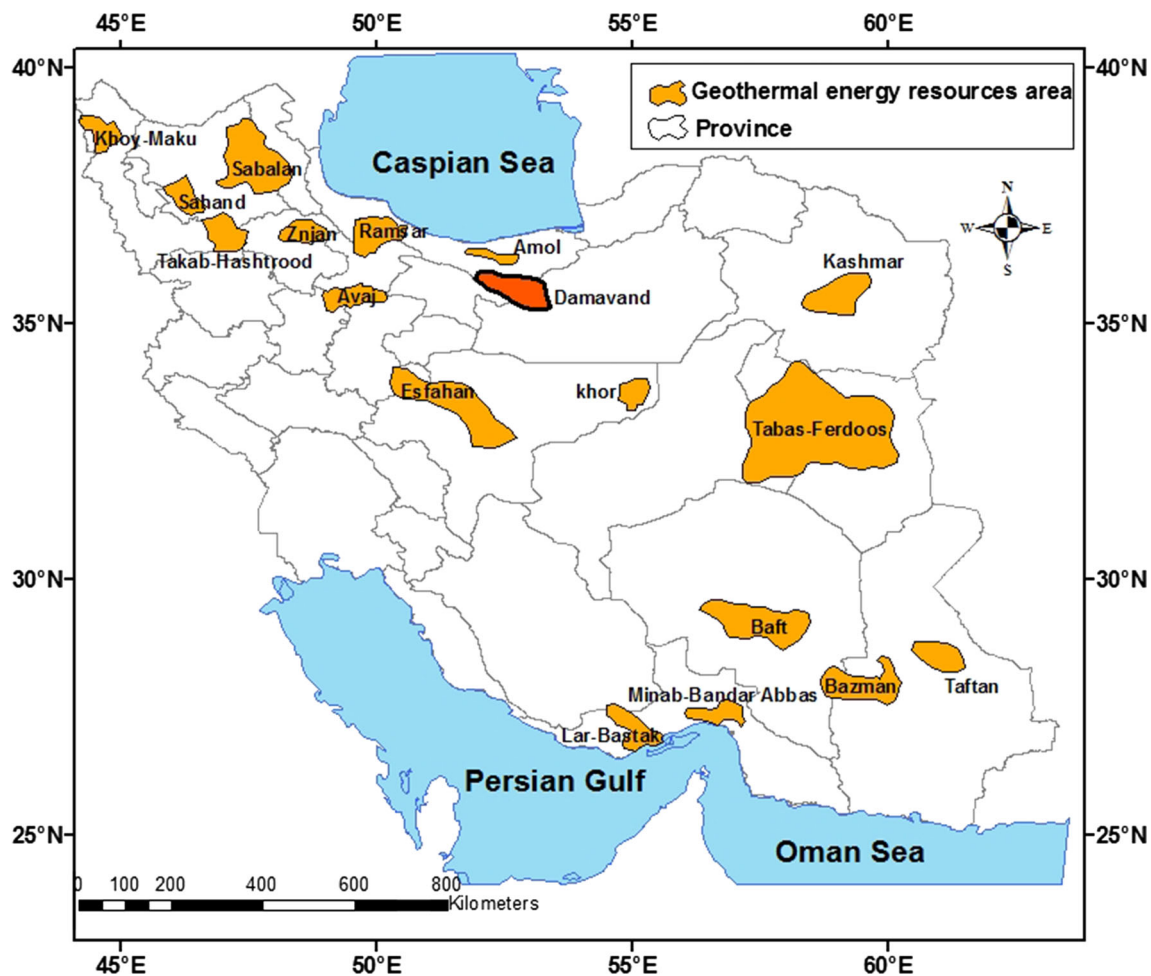
**Fig. 2** Geothermal energy resources map of Iran with the study area highlighted in red (adopted from Yousefi et al. 2007)

reservoir rock geology (faulted carbonate lithology), including Semnan spas. They determined that diffuse recharge and deep infiltration of meteoric water and long contact with Jeirud carbonate Formation (Upper Devonian) caused this water facies. Semnan thermal springs are located on the southern flank of the Alborz Mountain Range (Fig. 3). The thermal springs emerge in the vicinity of Mehdishahr, 21 km northwest of Semnan. Tourists and local people use these springs for swimming and skin disease treatment. The remnants of some mud and adobe building that were probably baths and caravansary show usage of these springs from the pre-Islamic era.

The study area is situated in one of the 18 suggested geothermal areas in the geothermal potential map of Iran (Yousefi et al. 2007, 2010). Prior to this study, no detail work had been done on the thermal springs of Semnan. The regional water company of Semnan carried out a preliminary study on these springs and contended that carbonate formation outcropping in the surrounding mountains is possibly the springs recharging area. Recognition of the reservoir temperature and the source of these springs will help in assessment of their potential for development of tourism, remedial and energy production.

In this paper, the physicochemical characteristics of groundwater and Semnan thermal springs are used to elucidate: (1) the origin of thermal springs and their most probable recharge areas, (2) the likely temperature of the heating reservoir of the thermal springs and (3) hydrogeochemical processes controlling the chemistry of the thermal water.

### Geological setting

From the perspective of Iran's plateau tectonics, the study area falls in the Alborz zone (Alavi 1991). Alborz Mountain Range runs from west to east, from the border of Azerbaijan, along the western and southern coast of the Caspian Sea, to Kopet Dagh Mountains in the northeast of Iran. Alborz Mountain Range is divided into western, central and eastern parts based on its structural geology. The study area is a part of the central and eastern Alborz Mountains (Fig. 1). The general trend of geological
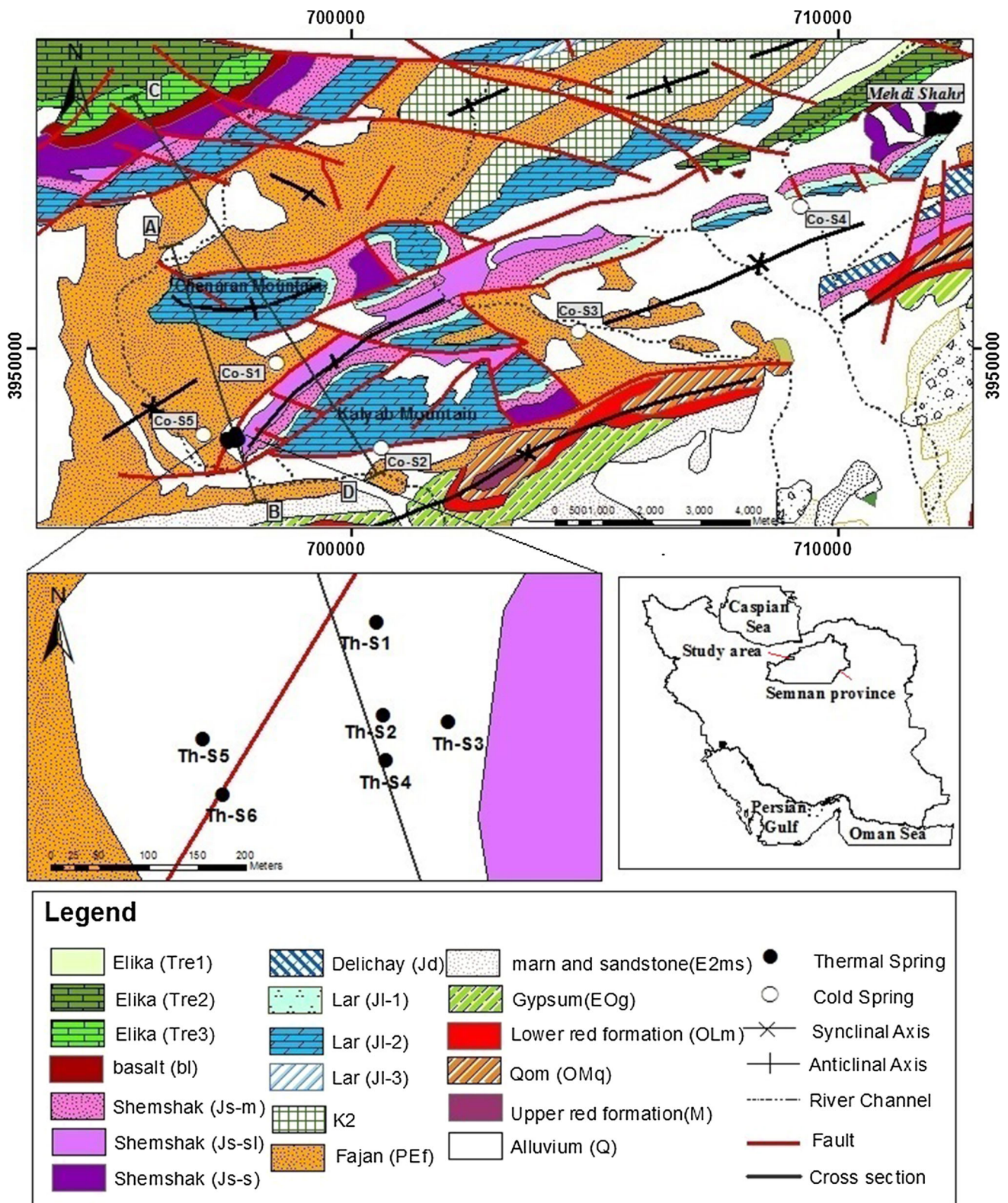
**Fig. 3** Geological map of the study area and location of the sampling points (modified from Nabavi 1987)

structures such as folding, faulting and rock strata in the study area follows NE–SW trend of the eastern Alborz. The study area is tectonically an active area, and the most important tectonic characteristic of this area is faulting. The most important active faults in the area include Semnan, Diktash, Anzab, Goleroodbar and Bashm faults

(Fig. 3). The major geologic formations outcropping in the study area (Fig. 3), in increasing order of age, are Elika Formation (Lower to Middle Triassic), Shemshak Formation (Lower Jurassic), Lar Formation (Middle to Late Jurassic), Fajan Formation (Paleocene–Eocene) and recent alluvium. Detailed lithological descriptions of stratigraphic units are presented in Table 1 (Darvishzade 1991; Nabavi 1976; Stöcklin and Setudehnia 1991).

Elika Formation (abbreviated with Tre in Table 1 and Figs. 3, 4) is divided into three members: lower (Tre1), middle (Tre2) and upper members (Tre3), which consist of dolomite and vermicular limestone, thick-bedded dolomite, and white limestone, respectively. The upper member is named as Versek member. Shemshak Formation (abbreviated with Js in Table 1) overlies the Elika Formation by an unconformity. The Shemshak Formation is made of sandstone, shale, marl and thin limestone and minor coal deposits. Shemshak Formation has been subdivided into several members: Diktash member (Js-m) (marl, shale and rare sandstone), Shahmirzad member (Js-sl) (sandstone, sandy limestone and Calcareous shale), Tazareh member (Js-s) (sandstone, shale, few coal seams and limestone beds) and basalt and ferruginous member (bl) (basalt and laterite). The Shemshak Formation is followed by the Lar Formation. Lithologically, the Lar Formation (abbreviated with Jl in Table 1) is divided into three members: The underside unit (Jl-1) consists of thin layers of limestone with abundant chert bands and nodules and Ammonite fossils. The middle part (Jl-2) is the main section, and it is characterized by thick dolomitic layers up to 1.5 m that become massive dolomite, and the upper section (Jl-3) consists of limestone layers with

little expanse. The outcrop of this member is just to the north of Semnan City. The continental conglomerates and red sandstones of Fajan Formation (abbreviated with PEf in Table 1) overlie the ancient folded Mesozoic Formations with angular unconformity due to the Laramide orogeny (Shahidi et al. 2008). Quaternary deposits are youngest sediments in this region and include young flood sediments (Qal) in the path of rivers and channels.

## Hydrogeological setting

The study area is a part of a regional synclinal structure that contains several folds and anticlines as a result of active tectonics in the region. The Elika and Lar Formations outcropping in the high altitude in the study area favor an important water recharge area and create the essential hydraulic gradient driving the groundwater fluxes from the higher altitude to the lower parts of the syncline. It seems that the general direction of groundwater flow is from north to south according to the topographic gradient and discharging point of the springs (see Fig. 4) for the geological cross section. The Elika Formation lies in syncline at depth; because of very thick impermeable layers of the Shemshak Formation there is no hydraulic connection between the carbonate aquifers of Elika and Lar Formations (Fig. 4). So the middle unit of the Lar Formation is the main aquifer in the study area. Although several faults cut the areal continuity of Lar Formation, its extensive outcrop is a potential recharge area of precipitation. Although pumping test has not been done in this area for the evaluation of the aquifer hydrodynamic coefficients, the

**Table 1** Simplified stratigraphic column of the study area

| Age | Hydrostratigraphic units | Lithostratigraphic units | Members | Lithological description |
|-----|--------------------------|--------------------------|---------|--------------------------|
| Quaternary | Permeable | Alluvium (Q) | | Young flood sediment |
| Paleocene–Eocene | Impermeable/semi-permeable | Fajan Formation (PEf) | – | Continental conglomerates and red sandstones |
| Middle to Late Jurassic | Permeable | Lar Formation (Jl) | Upper (Versek) | White limestone |
| | | | Middle | Thick-bedded dolomite |
| | | | Lower | Thin layers of limestone with abundant chert bands and nodules and Ammonite fossils |
| Lower Jurassic | Impermeable/semi-permeable | Shemshak Formation (Js) | Diktash member | Marl, shale and rare sandstone |
| | | | Shahmirzad member | Sandstone, sandy limestone and calcareous shale |
| | | | Tazareh member | Sandstone, shale, few coal seams and limestone beds |
| | | | Basalt and ferruginous member | Basalt and laterite |
| Lower to Middle Triassic | Permeable | Elika Formation (Tre) | Upper | White limestone |
| | | | Middle | Thick-bedded dolomite |
| | | | Lower | Dolomite and vermicular limestone |
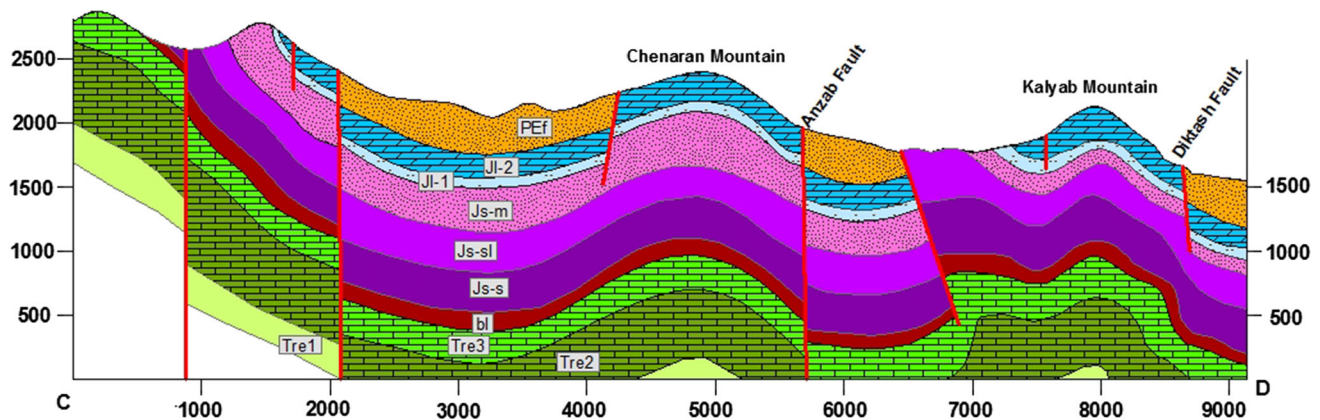
**Fig. 4** Geological cross sections along C–D in Fig. 3

secondary widening of the joints by dissolution, numerous bedding plains and faults could provide reliable permeability and water storage in a likely fractured karst aquifer.

Annual precipitation is the main source of groundwater recharge in the study area. There is no permanent surface water body such as river or lake except the Abgarm River which originates from thermal springs. The study area located in arid to semi-arid regions with an average annual precipitation and temperature of 140 mm and 18 °C, respectively, based on Semnan meteorological station which is located at an altitude of 1095 m above mean sea level (AMSL). The average minimum and maximum daily temperatures are about 4 and 31 °C in January and July, respectively, in the 40-year period of 1966–2005. Natural annual recharge occurs through outcrops of the carbonate formations of the Chenaran and Kelyab Mountains in highlands. Beyond the recharge area, the carbonate aquifer is covered by thick and less permeable layers of Fajan Formation and a confined aquifer condition is created (Fig. 4). Two groups of springs including thermal and cold springs were identified in the study area based on the preliminary measurements of groundwater temperature.

Like other geothermal systems in Iran (Mohammadi and Parizi 2013; Kompani-Zare and Moore 2001; Karimi and Moore 2008), the main discharge path of deep thermal water is along the major faults. The thermal springs emerge from different outlet points, labeled as Th-S1, Th-S2, Th-S3, Th-S4, Th-S5 and Th-S6 with the mean annual discharge of 5.4, 0.75, 0.2, 6.7, 3.0 and 2.5 l/s, respectively (Fig. 3). In the mid-1970s two large swimming pools were built, to store the Th-S1 and Th-S2 springs water for bathing and medical purposes (Fig. 3). Spring Th-S3 discharges to a small concert pit in the east of the Th-S2. Spring Th-S4 emerges at the foot of pool Th-S2 from a natural aqueduct. Th-S5 and Th-S6 discharge to a natural pool 200 m west of the other four thermal springs (Fig. 3).

The outlet elevations of Th-S1–4 and Th-S5–6 are 1633 and 1620 m AMSL, respectively.

Five cold springs emerge in the study area (Fig. 3). Spring Co-S1 with a mean annual discharge rate of 0.8 l/s is situated 2 km NE of the thermal springs and at the elevation of 1741 m AMSL. Spring Co-S1 discharges from the red sandstone of Fajan Formation, and the rock falls adjacent the southern flank of Chenaran Mountain (Fig. 3). Spring Co-S2 with a discharge rate of 1.5 l/s emerges 3 km SE of thermal springs from the karstic Lar Formation at the contact of Fajan and Lar Formations by Diktash thrust fault. Spring Co-S3 with a discharge of 0.2 l/s emerges at the contact of Fajan and Shemshak Formations. Spring Co-S4 with a discharge of 170 l/s located 3 km SW of Mehdishahr City at the elevation of 1551 m AMSL emerges from carbonate formations. Spring Co-S5 emerges from Fajan Formation at the elevation of 1623 m AMSL about 600 m west of Th-S5–6 thermal springs.

## Method of study

Groundwater samples of the six thermal springs with five shallow cold springs (Fig. 3) were collected during two surveys in January and April 2015 for analysis of the major anions and cations. Water sampling for measurement of minor and trace elements was carried out for all the thermal and cold springs in January 2015 and only for the thermal springs in April 2015. For trace metal analysis, water was filtered through 0.45-µm filters into prewashed 60-ml dark polyethylene bottle and immediately acidified to pH < 2 by the addition of Merck ultrapure nitric acid and stored at a temperature of < 4 °C until analyses.

The samples were analyzed in the laboratory of Semnan Regional Water Company for their chemical constituents using the following methods: The concentration of Ca, Mg,

Cl and $HCO_3$ was measured by titration using EDTA, 0.02 N, $H_2SO_4$ and $AgNO_3$, respectively. The concentration of Na and K was determined using a flame photometer. The concentration of $SO_4$, F and $SiO_2$ was determined using a spectrophotometer. Water samples were diluted with distilled water to achieve optimal analytical range. Trace and minor elements were determined by ICP-MS. The electric conductivity (EC), water temperature and pH of the water samples were measured on-site.

Discharge of the springs was measured using the flumes and/or volumetric method. General characteristics of the springs are presented in Tables 2 and 3. The ion balance is in the range of 0–7.87% (Table 2). The reaction error was less than 5% in most of the analyses except the spring Th-S5 which has high salinity. The dilution of the spring Th-S5 samples with distilled water and the use of unfiltered water sample may be the reason. In addition, precipitation/outgassing or non-measured constituents may also be the cause of error.

The PHREEQC software (Parkhurst and Appelo 1999) and the AquaChem code (Calmbach 1997) were used to calculate the mineral saturation indices and for the classification and evaluation of chemical properties of the water samples.

## Results

### Major ions

Water temperature of the thermal waters ranges between 20.9 and 35.1 °C (Table 2). Total dissolved solids (TDS) of the samples range from 9460 to 11,580 mg/l (Table 2). The acidity of the thermal waters is near neutral with high EC ranging from 14,200 to 17,380 μS/cm (Table 2). The ratios of Cl concentration to total anions and Na concentration to total cations in the thermal waters vary from 74.8 to 81.39% and 75.72 to 81.04% meq as the predominant major anion and cation, respectively.

The TDS of cold springs were lower (from 346 to 3060 mg/l) than that of the thermal springs. The electrical conductivity of the cold springs ranges between 520 and 4570 μS/cm. pH of the cold springs ranges from 7.64 to 8.42, and the temperature varies from 9.8 to 23.2 °C (Table 2).

The semi-logarithmic Schoeller plot shows that thermal and cold springs have a different chemical composition (Fig. 5). The trend of the major cations and anions in the cold waters is $Mg > Na > Ca$ and $SO_4 > HCO_3 > Cl$, respectively, while the thermal springs follow the trend of $Na > Ca > Mg$ and $Cl > SO_4 > HCO_3$. A small variation of $HCO_3$ shows the similarity of the dissolution of carbon dioxide in the all samples of the study area. On the other hand, the similar chemical composition of the thermal springs and their sulfurous smell may indicate single thermal reservoir. Even though thermal springs Th-S5 and Th-S6 with the average water temperature of 28.6 and 28.05 °C, respectively, present similar geochemical signatures, their average TDS values (11,215 and 11,480 mg/l, respectively) are higher than that of other thermal springs (Table 2). Based on the similar chloride concentrations especially in the first four studied thermal springs, thermal waters with different temperatures are cooled mainly by conductive heat loss (Fournier 1979).

The linear relationship between Cl and EC, temperature, and some major cations such as Na, K, Mg, Ca and some minor elements such as F and $SiO_2$ is illustrated in Fig. 6. Variations of Cl correlate with water temperature (Fig. 6a), $R^2 = 0.7$, and indicate that the temperature-related water–rock interaction affected the chemical composition of waters. The general sequence as outlined by Chebotarev (1955) involves the passage of bicarbonate water type in the shallow ground water system to chloride water type at greater depths of travel with increasing time of contact with the aquifer rocks (Fig. 7). Probably, accumulations of Na and Cl in the crystal lattice of minerals in Lar Formation cause an increase in these two ions in karstic Co-S4. However, Co-S2 with a little discharge shows a low concentration of sodium and chloride ions. It seems that lower resident time of groundwater flow through probable faults prevents raising of the ion concentrations in this spring.

Co-S5 with higher EC and dissolved ion concentrations shows lower temperature. The dissolution of Na-feldspar and K-feldspar of Fajan Sandstone Formation may cause increasing Na, K and $SiO_2$ concentrations. Higher Ca and $SO_4$ concentration in this spring (Table 2) is commonly attributed to dissolution of the gypsum lenses in Fajan Formation. In general, lower concentration of trace elements and major ions content in the cold spring water is due to shorter transit pathway and shorter resident time and hence limited water–rock interaction due to a shallow percolation depth (Chandrajith et al. 2013).

### Minor and trace elements

The thermal spring waters were characterized by the elevated concentration of Sr, F, $SiO_2$, Li, Rb, Cs. An increase in the concentration of the minor and trace elements in the thermal waters is attributed to water–rock interaction in higher temperature and longer residence time (Fig. 6g, h) (Tarcan and Gemici 2003; Han et al. 2010; Alçiçek et al. 2016; Langmuir 1997).

A small variation in concentrations of minor and trace elements between the thermal springs (Fig. 8) suggests that a common reservoir feeds them. The higher level of Li, Rb and Cs (Table 3), which are conservative, especially in the

**Table 2** Discharge and physicochemical characteristics of the water samples

| Samples | Date | Concentration (mg/l) | | | | | | | | I.B. (%) | EC (µS/cm) | pH_lab | pH_field | Temp (°C) | Q (l/s) |
|---|---|---|---|---|---|---|---|---|---|---|---|---|---|---|---|
| | | TDS | HCO$_3$ | Cl | SO$_4$ | Mg | Ca | Na | K | | | | | | |
| Thermal springs | | | | | | | | | | | | | | | |
| Th-S1 | 23.1.2015 | 9480 | 231.86 | 4440.49 | 1828.06 | 153.12 | 448.87 | 2673.05 | 64.12 | 4.44 | 14,230.00 | 7.06 | 7.02 | 28.20 | 8.04 |
| | 25.4.2015 | 9600 | 198.30 | 4484.80 | 1374.65 | 143.40 | 476.93 | 2999.97 | 66.86 | 2.89 | 14,420.00 | 6.76 | 6.93 | 33.50 | 4.39 |
| Th-S2 | 23.1.2015 | 9540 | 231.86 | 4564.57 | 1867.45 | 157.98 | 456.89 | 2684.54 | 64.12 | 5.29 | 14,370.00 | 7.39 | 7.48 | 20.90 | 0.62 |
| | 25.4.2015 | 9730 | 198.30 | 4484.80 | 1449.10 | 145.83 | 484.94 | 2999.97 | 68.81 | 2.60 | 14,620.00 | 6.82 | 7.09 | 28.70 | 0.62 |
| Th-S3 | 23.1.2015 | 9480 | 244.06 | 4475.94 | 1851.11 | 150.69 | 452.88 | 2689.14 | 64.12 | 4.71 | 14,230.00 | 6.93 | 6.89 | 32.10 | 0.19 |
| | 25.4.2015 | 9580 | 198.30 | 4449.35 | 1561.49 | 138.54 | 480.94 | 3099.74 | 73.90 | 3.26 | 14350.00 | 6.67 | 6.85 | 33.40 | 0.20 |
| Th-S4 | 23.1.2015 | 9460 | 244.06 | 4511.39 | 1649.86 | 153.12 | 448.87 | 2689.14 | 64.12 | 4 | 14,200.00 | 7 | 7 | 33 | 7 |
| | 25.4.2015 | 9560 | 189.15 | 4449.35 | 1512.02 | 131.25 | 492.96 | 2999.97 | 69.99 | 2.32 | 14,360.00 | 6.64 | 6.81 | 35.10 | 6.35 |
| Th-S5 | 23.1.2015 | 11,140 | 286.78 | 5521.80 | 1959.18 | 188.36 | 390.76 | 3097.67 | 83.28 | 7.87 | 16,730.00 | 7.13 | 7.10 | 28.20 | 3.10 |
| | 25.4.2015 | 11,290 | 225.76 | 5512.94 | 1529.79 | 148.26 | 488.95 | 3810.36 | 84.84 | 3.40 | 16,950.00 | 6.70 | 7.08 | 29.00 | 3.12 |
| Th-S6 | 23.1.2015 | 11,380 | 283.72 | 5645.89 | 1699.34 | 182.29 | 390.76 | 3398.38 | 86.02 | 3.85 | 17,080.00 | 7.10 | 7.17 | 27.10 | 2.05 |
| | 25.4.2015 | 11,580 | 231.86 | 5707.93 | 1852.56 | 150.69 | 484.94 | 3810.36 | 93.84 | 0.34 | 17,380.00 | 6.72 | 7.05 | 29.00 | 2.10 |
| Cold springs | | | | | | | | | | | | | | | |
| Co-S1 | 23.1.2015 | 509 | 237.96 | 34.74 | 224.30 | 44.96 | 42.08 | 54.95 | 4.30 | 7.08 | 767.00 | 7.89 | 7.95 | 15.10 | * |
| | 25.4.2015 | 529 | 222.71 | 29.07 | 210.38 | 38.89 | 54.11 | 64.14 | 4.30 | 0 | 795.00 | 8 | 8 | 22 | 0.79 |
| Co-S2 | 23.1.2015 | 346 | 207.45 | 23.40 | 75.41 | 32.20 | 34.07 | 28.51 | 1.95 | 0.09 | 520.00 | 7.73 | 7.70 | 20.00 | * |
| | 25.4.2015 | 346 | 192.20 | 21.98 | 89.34 | 25.52 | 44.09 | 28.97 | 2.74 | 0.00 | 521.00 | 7.71 | 7.77 | 22.70 | 1.47 |
| Co-S3 | 23.1.2015 | 870 | 228.81 | 86.86 | 427.96 | 67.45 | 70.14 | 125.07 | 4.30 | 3.66 | 1306.00 | 8.23 | 8.39 | 12.90 | * |
| | 25.4.2015 | 878 | 234.91 | 86.86 | 427.00 | 60.76 | 80.16 | 157.94 | 4.30 | 2.53 | 1321.00 | 7.69 | 8.33 | 20.50 | 0.17 |
| Co-S4 | 23.1.2015 | 937 | 259.32 | 241.08 | 190.68 | 48.61 | 64.12 | 156.10 | 4.69 | 3.12 | 1406.00 | 7.56 | 7.64 | 18.20 | 170.00 |
| Co-S5 | 23.1.2015 | 2790 | 259.32 | 219.81 | 2626.82 | 267.36 | 296.58 | 434.74 | 32.06 | 7.08 | 4190.00 | 7.85 | 8.24 | 9.80 | * |
| | 25.4.2015 | 3060 | 158.64 | 255.26 | 2857.84 | 269.79 | 344.67 | 632.00 | 32.84 | 1.15 | 4570.00 | 7.48 | 8.42 | 23.20 | 0.1** |

* Not measured

** Estimated discharge (not measured)

**Table 3** Concentrations of minor and trace elements in the water samples

| Samples | Date | Concentration (µg/l) | | | | | | | | | | | |
|---|---|---|---|---|---|---|---|---|---|---|---|---|---|
| | | $SiO_2$ | Sr | Rb | Cs | Li | Fe | Mn | Ba | Al | Cr | Ni | Cd |
| Thermal springs | | | | | | | | | | | | | |
| Th-S1 | 23.1.2015 | 42.00 | 21.800 | 0.244 | 0.127 | 1.350 | 0.060 | 0.080 | 0.028 | 0.120 | 0.039 | 0.004 | 0.006 |
| | 25.4.2015 | 39.00 | 20.230 | 0.234 | 0.124 | 1.240 | 0.120 | 0.080 | 0.030 | 0.140 | 0.073 | 0.009 | 0.003 |
| Th-S2 | 23.1.2015 | 43.00 | 21.570 | 0.238 | 0.126 | 1.300 | 0.070 | 0.080 | 0.027 | 0.120 | 0.022 | 0.002 | 0.002 |
| | 25.4.2015 | 38.00 | 22.580 | 0.258 | 0.134 | 1.410 | 0.140 | 0.080 | 0.033 | 0.170 | 0.082 | 0.010 | 0.003 |
| Th-S3 | 23.1.2015 | 41.00 | 21.110 | 0.238 | 0.125 | 1.290 | 0.080 | 0.080 | 0.022 | 0.130 | 0.016 | 0.001 | 0.003 |
| | 25.4.2015 | 38.00 | 21.600 | 0.247 | 0.128 | 1.350 | 0.140 | 0.080 | 0.026 | 0.150 | 0.095 | 0.011 | 0.002 |
| Th-S4 | 23.1.2015 | 44.00 | 23.260 | 0.263 | 0.139 | 1.460 | 0.060 | 0.080 | 0.026 | 0.130 | 0.017 | 0.003 | 0.003 |
| | 25.4.2015 | 39.00 | 21.710 | 0.263 | 0.140 | 1.360 | 0.150 | 0.080 | 0.028 | 0.140 | 0.085 | 0.010 | 0.003 |
| Th-S5 | 23.1.2015 | 44.00 | 22.250 | 0.334 | 0.160 | 1.640 | 0.110 | 0.090 | 0.022 | 0.140 | 0.083 | 0.010 | 0.002 |
| | 25.4.2015 | 38.00 | 23.920 | 0.308 | 0.157 | 1.770 | 0.180 | 0.100 | 0.023 | 0.150 | 0.107 | 0.010 | 0.002 |
| Th-S6 | 23.1.2015 | 43.00 | 23.420 | 0.300 | 0.152 | 1.780 | 0.070 | 0.090 | 0.022 | 0.120 | 0.018 | 0.005 | 0.002 |
| | 25.4.2015 | 39.00 | 23.690 | 0.304 | 0.153 | 1.800 | 0.150 | 0.090 | 0.026 | 0.140 | 0.084 | 0.010 | 0.002 |
| Cold springs | | | | | | | | | | | | | |
| Co-S1 | 23.1.2015 | 16.00 | 1.440 | 0.009 | 0.000 | 0.040 | 0.060 | UDL | 0.023 | 0.050 | 0.025 | 0.007 | 0.003 |
| | 25.4.2015 | 14.00 | * | * | * | * | * | * | * | * | * | * | * |
| Co-S2 | 23.1.2015 | 15.00 | 1.000 | 0.005 | 0.000 | 0.020 | 0.060 | UDL | 0.021 | 0.050 | 0.041 | 0.007 | 0.002 |
| | 25.4.2015 | 12.00 | * | * | * | * | * | * | * | * | * | * | * |
| Co-S3 | 23.1.2015 | 11.00 | 3.210 | 0.005 | UDL | 0.060 | 0.150 | UDL | 0.012 | 0.060 | 0.056 | 0.008 | 0.003 |
| | 25.4.2015 | 16.00 | * | * | * | * | * | * | * | * | * | * | * |
| Co-S4 | 23.1.2015 | 12.00 | 2.280 | 0.010 | 0.002 | 0.100 | 0.070 | UDL | 0.024 | 0.060 | 0.037 | 0.004 | 0.003 |
| Co-S5 | 23.1.2015 | 17.00 | 16.130 | 0.010 | UDL | 0.550 | 0.110 | 0.020 | 0.010 | 0.150 | 0.040 | 0.007 | 0.003 |
| | 25.4.2015 | 23.00 | * | * | * | * | * | * | * | * | * | * | * |

*UDL* under detection limit

* Not measured

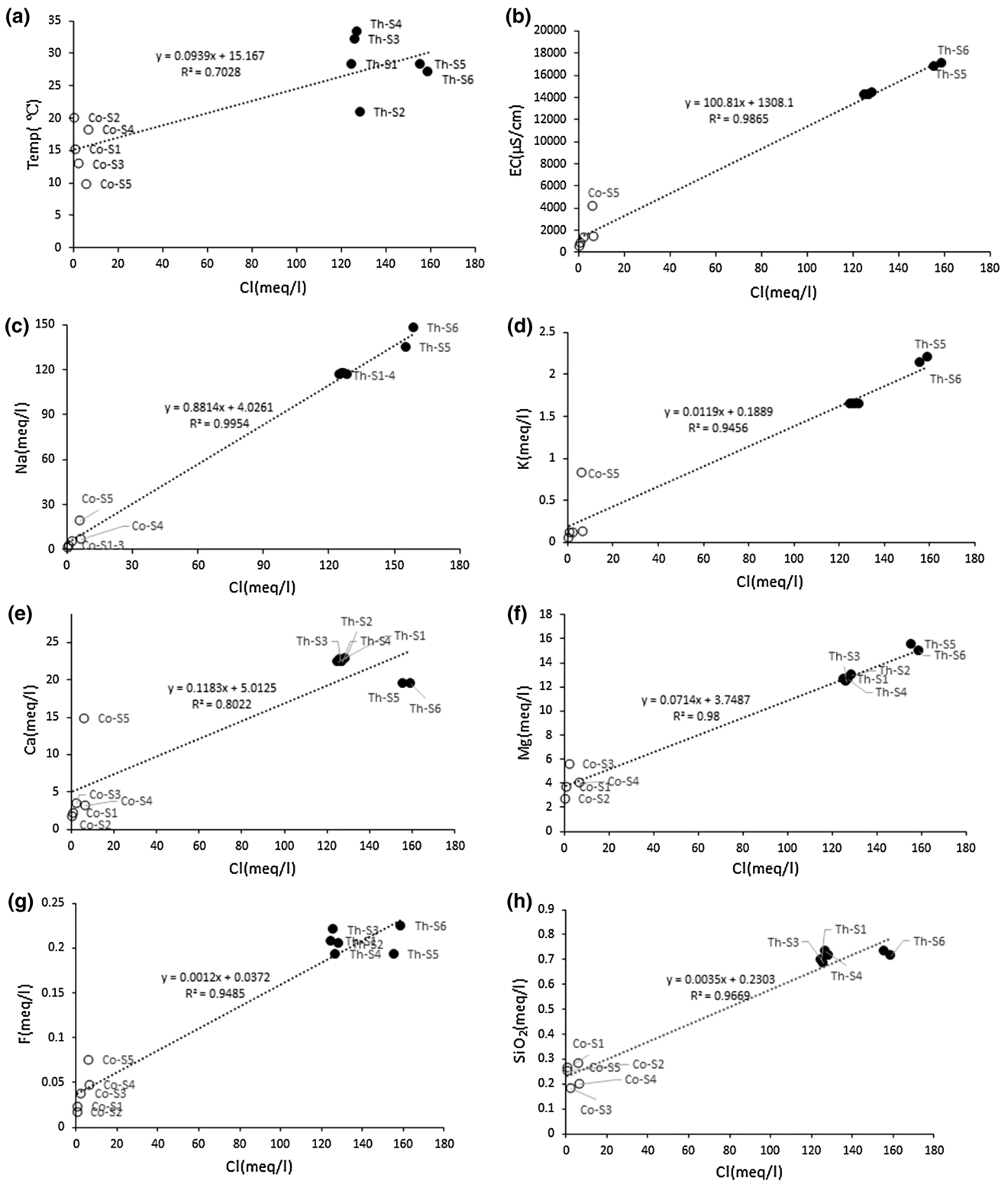**Fig. 5** Semi-logarithmic Schoeller diagram for the springs
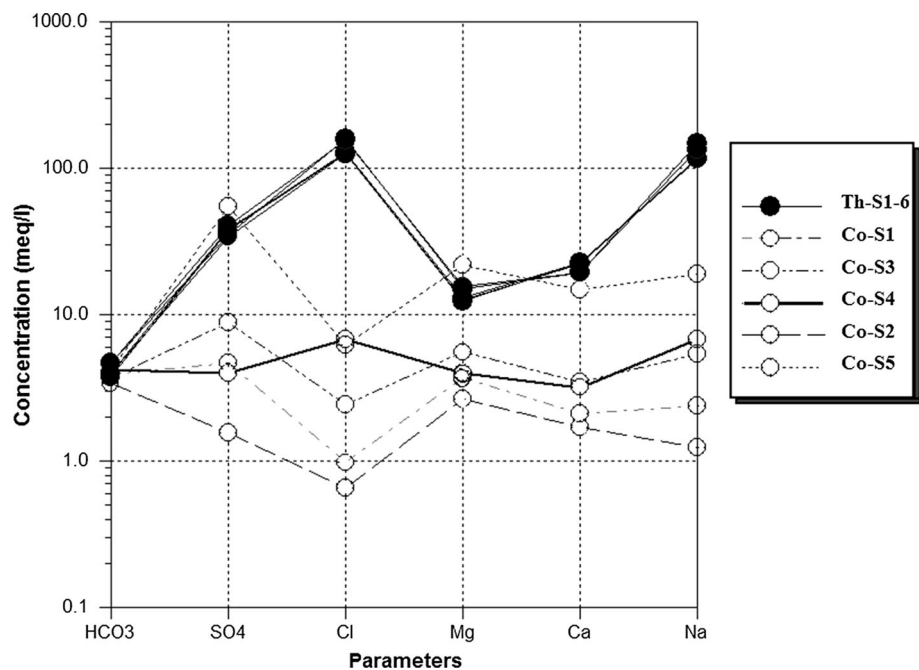
**Fig. 6** Relationship between chloride and the various ions: **a** K versus Cl, **b** EC versus Cl, **c** Na versus Cl, **d** K versus Cl, **e** Ca versus Cl, **f** Mg versus Cl, **g** F versus Cl, **h** $SiO_2$ versus Cl

thermal springs Th-S5 and Th-S6, with higher total dissolved minerals, is probably due to the longer residence time and circulation depth.

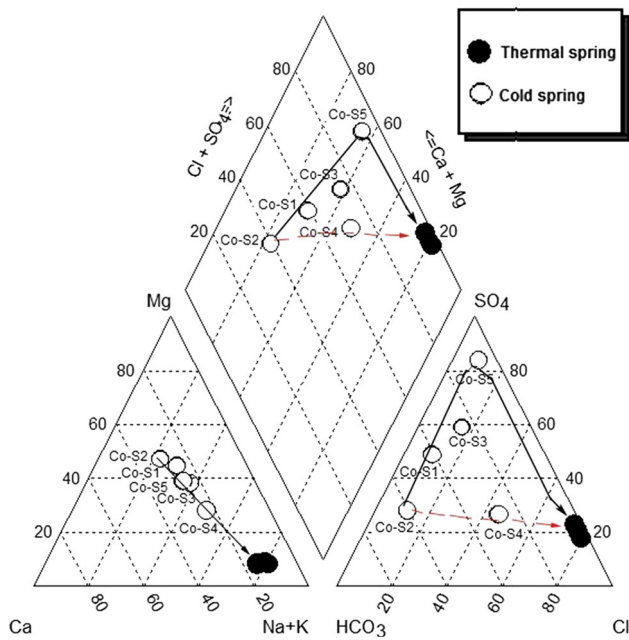Comparing the analysis of trace elements in both wet and dry seasons shows no significant changes in the concentration of the most elements. However, some trace

**Fig. 7** Trilinear diagram of Piper for thermal and cold springs in January (the arrows represent the path that the water could follows to reach the thermal waters)

elements including iron, chromium and nickel in April increases about two orders of magnitude. Szczucińska et al. (2010) attributed a twofold increase in iron in groundwater outflows (springs and seeps) from porous sediments in the Gryżyna-Grabin Tunnel Valley in western Poland to the seasonal variation of pH, temperature and the availability of oxygen. $Fe^{2+}$ precipitates in alkaline and oxidation conditions, whereas it is soluble in acid and reducing conditions. It seems that the reduction in pH in April causes an increase in the dissolution of iron and trace elements with similar behavior such as chromium and nickel (Kabata-Pendias and Mukherjee 2007). On the other hand, dilution effect of precipitation in wet period may

provoke the lower concentration of these trace elements in January.

## Chemical geothermometry

Chemical geothermometry is a principal method used in the exploration of geothermal resources (Karingithi 2009). Silica and cation geothermometers are the most used geothermometers for the estimation of the reservoir temperature. The first one is based on absolute concentration and variation in solubility of silica with temperature, and the second one is based on concentration ratios and temperature dependence of equilibrium state for exchange of some cations between the associated host rocks and solution. The calculated reservoir temperatures from the all studied springs using various chemical geothermometers are presented in Table 4.

For the evaluation of the chemical equilibrium of thermal springs and its suitability for estimating reservoir temperature, the triangular equilibrium and Na–K–Ca–Mg plot of Giggenbach (1988) and Giggenbach and Glover (1992) were used (Figs. 9, 10). The thermal samples plot away from the equilibrium line, and their Mg concentration suggests that thermal waters are partially in equilibrium with the host rocks, or they re-equilibrated after mixing with cold waters, and their temperature changed during these processes. For these waters, the temperature of geothermal reservoirs can be estimated by K/Mg geothermometer (Giggenbach 1988). The acquisition of Mg by the water with the decreasing temperatures is faster than that of Na and Ca (Nicholson 1993). So the estimated reservoir temperature of the study area based on the K/Mg geothermometer is about 80 °C, which is lower than the estimated temperature by the Na/K geothermometer (140 °C).

As shown in Table 4, the Na/K geothermometer (Giggenbach 1988), Na–K–Ca (Fournier and Truesdell 1973) and Mg/Li (Kharaka and Mariner 1989) give high reservoir temperature, while the results of Na/Li (Fouillac
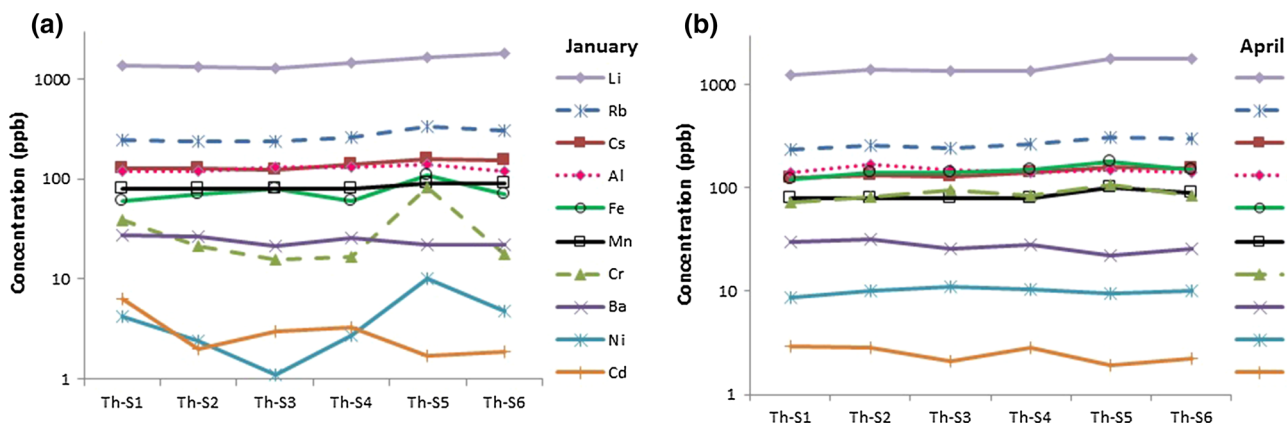


**Fig. 8** Spatial variation of the logarithmic concentration of trace elements in thermal spring in **a** wet (January) and **b** dry (April) seasons
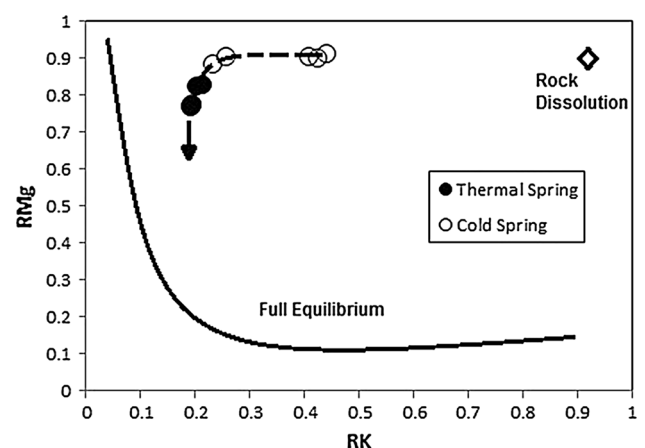
**Table 4** Estimated geothermal reservoir temperatures (°C) using chemical geothermometers

| Geothermometer | Water samples | | | | | | | | | | | |
|---|---|---|---|---|---|---|---|---|---|---|---|---|
| | Th-S1 | | Th-S2 | | Th-S3 | | Th-S4 | | Th-S5 | | Th-S6 | |
| | January | April | January | April | January | April | January | April | January | April | January | April |
| Quartz—no-steam loss (Fournier 1977) | 94 | 91 | 95 | 89 | 93 | 89 | 96 | 91 | 96 | 89 | 95 | 91 |
| Quartz—Max steam loss (Fournier 1977) | 96 | 93 | 97 | 92 | 95 | 92 | 97 | 93 | 97 | 92 | 97 | 93 |
| Quartz (Arnorsson 1983) | 80 | 76 | 81 | 75 | 79 | 75 | 82 | 76 | 82 | 75 | 81 | 76 |
| Chalcedony (Fournier 1977) | 63 | 60 | 64 | 59 | 62 | 59 | 66 | 60 | 66 | 59 | 64 | 60 |
| Chalcedony (Arnorsson 1983) | 65 | 62 | 66 | 61 | 64 | 61 | 67 | 62 | 67 | 61 | 66 | 62 |
| Na–K–Ca (Fournier and Truesdell 1973) | 131 | 129 | 131 | 130 | 131 | 132 | 131 | 131 | 139 | 132 | 138 | 137 |
| Na/Li (Fouillac and Michard 1981) | 43 | 34 | 41 | 40 | 41 | 36 | 46 | 38 | 45 | 39 | 44 | 40 |
| K/Mg (Giggenbach 1988) | 142 | 139 | 142 | 139 | 141 | 135 | 142 | 136 | 136 | 132 | 135 | 129 |
| Mg/Li (Kharaka and Mariner 1989) | 347 | 355 | 356 | 337 | 353 | 340 | 336 | 335 | 334 | 307 | 320 | 305 |
| Na/K (Giggenbach 1988) | 519 | 519 | 519 | 519 | 519 | 519 | 519 | 519 | 519 | 519 | 519 | 519 |
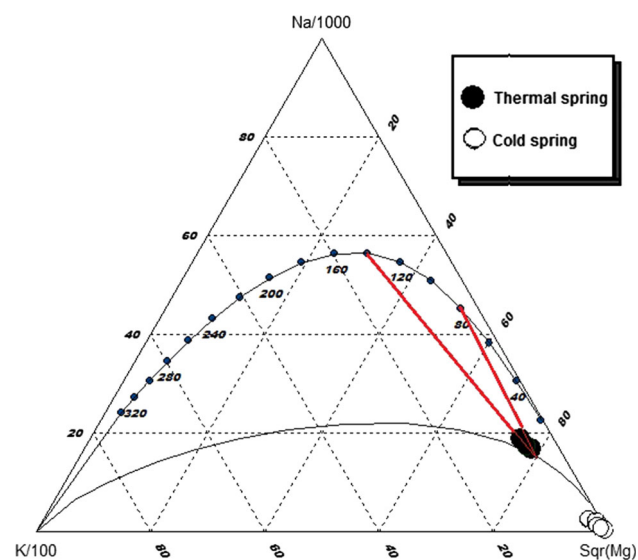


**Fig. 9** Na–K–Mg triangular diagram of the studied samples



**Fig. 10** Plot of RK = $10C_K/(10C_K + C_{Na})$ versus RMg = $10C_{Mg}/(10C_{Mg} + C_{Ca})$ for the studied thermal and cold springs, C in mg/kg. The arrow represents an evolution trend that the water could follow to reach the mineral equilibrium

and Michard 1981) are close to measured temperatures in the thermal springs. Consequently, these geothermometers are unreliable for the estimation of reservoir temperature of Semnan thermal springs.

The calculated temperatures using the no-steam loss (89–96 °C) and maximum steam loss (92–97 °C) quartz geothermometers of Fournier (1977) are similar, which indicates that separation of vapor from the springs has not occurred, or in other words, geothermal water samples undergo conductive cooling. The average temperature estimated using the quartz geothermometer proposed by

Arnorsson et al. (1983) is about 78 °C. Although the temperatures calculated with these methods are different, this difference is admissible for geothermometry calculations with the typical uncertainty range of ± 20 °C (Asta et al. 2012).

The average thermal reservoir temperature calculated with chalcedony geothermometers is in the range of 59–67 °C. These results are in agreement with saturation index calculations shown in Fig. 11 and are about 20–30 °C lower than those calculated by quartz geothermometers.

**Fig. 11** Saturation state for some minerals of Th-S1 versus temperature in January
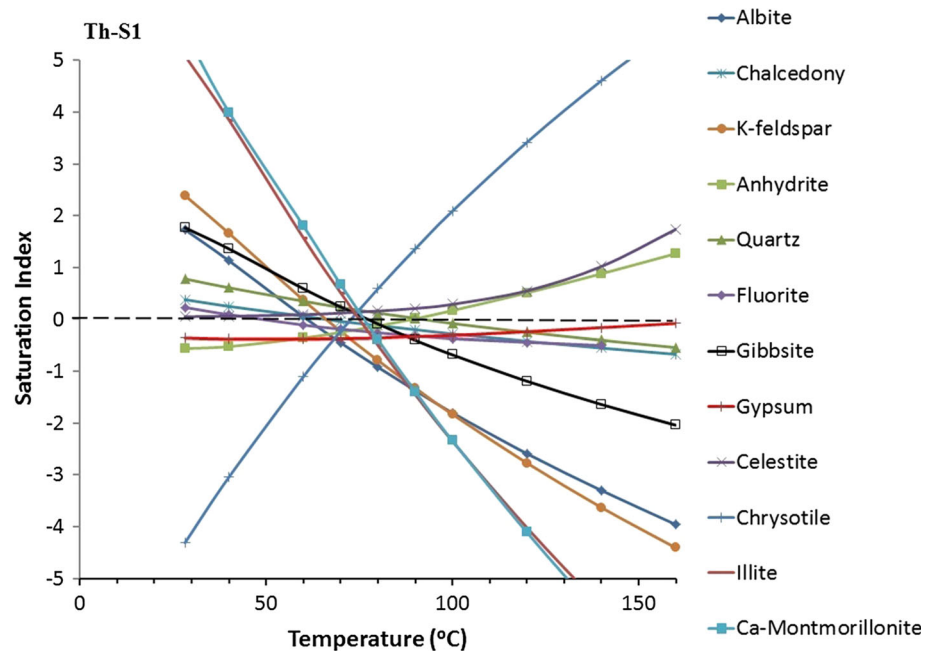
## Chemical equilibria

The saturation index (SI) is expressed by:

$$SI = \log\left(IAP/K_T\right), \tag{1}$$

where IAP is the ion activity product and $K_T$ is the thermodynamic equilibrium constant of the mineral under the temperature of the sampling spring.

The PHREEQC code (Parkhurst and Appelo 1999) was used to calculate the saturation index of minerals that were suspected to be responsible for the observed chemical composition of the spring water (Table 5). The studied thermal waters are undersaturated with $Al(OH)_3(a)$, gypsum, siderite and anhydrite, anorthite, halite, pyrochlorite and $SiO_2(a)$ minerals. However, they are supersaturated with albite, alunite, fluorite, Ca-montmorillonite, calcite, celestite, chalcedony, dolomite, $Fe(OH)_3(a)$, gibbsite, goethite, hematite, illite, K-feldspar, K-mica, kaolinite and quartz minerals. These oversaturations reflect the long residence time of water at a lower temperature before emerging to the surface, and on the other hand, scaling problem at the time of thermal water usage is likely (Gokgoz and Tarcan 2006).

The equilibrium between water and many minerals is a function of temperature, pressure and, to a lesser extent, solubility. Of these, the temperature is the dominant factor in controlling reservoir fluid composition. So saturation index can be used to obtain the temperature of deep reservoir thermal solution. Although the full equilibration between a fluid and all the minerals in the host rock at a particular temperature may not be achieved (Zheng and Liu 1996; Zhang et al. 2015), according to the study published by Reed and Spycher (1984) if SIs of a group of minerals intersect the zero line at a specific temperature, the water sample can be regarded to be in full equilibrium with these minerals. So the obtained temperature will be the most probable equilibrated reservoir temperature (D'Amore et al. 1987; Majumdar et al. 2009; Mohammadi et al. 2010; Asta et al. 2012).

For each of the samples, by changing the temperature the saturation index was calculated. Only the spring Th-S1 in January is selected and described further (Fig. 11). The K-feldspar, chalcedony and albite intersect the saturation equilibrium line at about 60 °C. Quartz and kaolinite cut the saturation curve at 90 °C.

K-feldspar relative to albite intersects the saturation equilibrium line at higher temperatures and has more stability. At higher temperature, they are at undersaturation state, but at 90 °C these two minerals converge to each other. This situation enhances the solubility of these minerals with increasing temperature.

Anhydrite at 90 °C reaches the equilibrium state and at a lower temperature is in the subsaturation state. Gibbsite, illite and montmorillonite are at the supersaturation state to a temperature of 70 °C, and kaolinite remains at supersaturation state to 90 °C and it proves the existence of clay minerals at the thermal system.

$Al(OH)_3$, melanterite, magnetite, otavite, siderite, smithsonite, witherite, halite and gypsum with increasing temperature are under saturation. In this case, increase in salinity and sodium concentration in the water due to an imbalance of these mineral continues. Fluorite is under saturation at a temperature of over 50 °C, and this suggests

**Table 5** Mineral saturation indices at two sampling time for the thermal springs

| Sample name | Th-S1 | | Th-S2 | | Th-S3 | | Th-S4 | | Th-S5 | | Th-S6 | |
|---|---|---|---|---|---|---|---|---|---|---|---|---|
| Date | January | April | January | April | January | April | January | April | January | April | January | April |
| $Al(OH)_3(a)$ | − 0.9 | − 0.88 | − 0.94 | − 0.75 | − 0.94 | − 0.84 | − 0.91 | − 0.88 | − 0.83 | − 0.81 | − 0.92 | − 0.83 |
| Albite | 1.73 | 1.45 | 2.36 | 1.85 | 1.43 | 1.43 | 1.51 | 1.32 | 2 | 1.89 | 2.02 | 1.88 |
| Alunite | 2.09 | 1.75 | 1.13 | 2.07 | 2.07 | 2.28 | 2.04 | 2.11 | 2.16 | 1.97 | 1.63 | 2.23 |
| Anhydrite | − 0.56 | − 0.64 | − 0.56 | − 0.63 | − 0.55 | − 0.59 | − 0.59 | − 0.58 | − 0.63 | − 0.64 | − 0.69 | − 0.58 |
| Anorthite | − 0.4 | − 0.35 | 0.1 | 0.01 | − 0.59 | − 0.43 | − 0.45 | − 0.49 | − 0.14 | − 0.11 | − 0.25 | − 0.19 |
| Aragonite | 0.04 | 0 | 0.4 | 0.1 | − 0.01 | − 0.09 | − 0.01 | − 0.11 | 0.13 | 0.13 | 0.19 | 0.09 |
| Barite | 0.11 | − 0.03 | 0.22 | 0.09 | − 0.05 | − 0.06 | 0 | − 0.05 | 0 | − 0.09 | − 0.03 | 0.02 |
| Ca-Montmorillonite | 5.54 | 5.12 | 6.01 | 5.72 | 5.15 | 5.2 | 5.28 | 5.04 | 5.79 | 5.58 | 5.63 | 5.59 |
| Calcite | 0.18 | 0.14 | 0.55 | 0.24 | 0.13 | 0.05 | 0.13 | 0.03 | 0.28 | 0.27 | 0.33 | 0.23 |
| $Cd(OH)_2$ | − 8.15 | − 8.68 | − 7.74 | − 8.37 | − 8.75 | − 8.98 | − 8.75 | − 9.1 | − 8.66 | − 8.64 | − 8.48 | − 8.66 |
| $CdSiO_3$ | − 6.56 | − 6.92 | − 6.43 | − 6.8 | − 7.01 | − 7.22 | − 6.94 | − 7.27 | − 7.04 | − 7.06 | − 6.91 | − 7.06 |
| $CdSO_4$ | − 10.73 | − 11.04 | − 11.48 | − 11.18 | − 10.93 | − 11.13 | − 10.91 | − 11.13 | − 11.39 | − 11.44 | − 11.45 | − 11.31 |
| Celestite | 0.05 | − 0.09 | 0.06 | − 0.03 | 0.04 | − 0.02 | 0.04 | − 0.03 | 0.05 | − 0.03 | 0.02 | 0.03 |
| Chalcedony | 0.38 | 0.28 | 0.48 | 0.34 | 0.33 | 0.28 | 0.35 | 0.28 | 0.41 | 0.34 | 0.41 | 0.35 |
| Chlorite(14A) | − 0.93 | − 0.75 | 1.99 | 0.06 | − 1.54 | − 1.63 | − 1.24 | − 1.81 | 0.45 | − 0.1 | 0.69 | − 0.45 |
| Chrysotile | − 4.31 | − 4.34 | − 2.35 | − 3.91 | − 4.71 | − 4.91 | − 4.58 | − 5.01 | − 3.56 | − 3.94 | − 3.28 | − 4.13 |
| $CO_2(g)$ | − 1.68 | − 1.62 | − 2.19 | − 1.82 | − 1.5 | − 1.54 | − 1.47 | − 1.51 | − 1.67 | − 1.76 | − 1.75 | − 1.71 |
| Dolomite | 0.28 | 0.19 | 0.94 | 0.35 | 0.19 | − 0.01 | 0.21 | − 0.08 | 0.62 | 0.42 | 0.72 | 0.35 |
| $Fe(OH)_3(a)$ | 0.53 | 0.66 | 1.58 | 1.08 | 0.35 | 0.52 | 0.19 | 0.47 | 0.96 | 1.15 | 0.93 | 0.99 |
| Fluorite | 0.23 | 0.11 | 0.34 | 0.17 | 0.23 | 0.1 | 0.11 | 0.06 | 0.07 | 0.15 | 0.23 | 0.12 |
| Gibbsite | 1.77 | 1.73 | 1.79 | 1.9 | 1.69 | 1.78 | 1.71 | 1.72 | 1.83 | 1.84 | 1.75 | 1.83 |
| Goethite | 6.53 | 6.85 | 7.33 | 7.1 | 6.49 | 6.71 | 6.37 | 6.71 | 6.97 | 7.18 | 6.9 | 7.02 |
| Gypsum | − 0.36 | − 0.46 | − 0.33 | − 0.43 | − 0.36 | − 0.41 | − 0.41 | − 0.41 | − 0.43 | − 0.45 | − 0.49 | − 0.38 |
| $H_2(g)$ | − 22.03 | − 21.83 | − 22.97 | − 22.17 | − 21.76 | − 21.67 | − 21.71 | − 21.59 | − 22.19 | − 22.15 | − 22.33 | − 22.09 |
| $H_2O(g)$ | − 1.43 | − 1.3 | − 1.62 | − 1.42 | − 1.33 | − 1.3 | − 1.31 | − 1.26 | − 1.43 | − 1.41 | − 1.46 | − 1.41 |
| Halite | − 3.7 | − 3.65 | − 3.66 | − 3.64 | − 3.7 | − 3.64 | − 3.7 | − 3.66 | − 3.55 | − 3.46 | − 3.49 | − 3.45 |
| Hausmannite | − 15.61 | − 15.01 | − 13.77 | − 14.87 | − 15.74 | − 15.69 | − 15.61 | − 15.61 | − 14.92 | − 14.68 | − 14.61 | − 15.1 |
| Hematite | 15.09 | 15.74 | 16.65 | 16.24 | 15.03 | 15.46 | 14.79 | 15.47 | 15.96 | 16.4 | 15.81 | 16.08 |
| Illite | 5.09 | 4.64 | 5.86 | 5.34 | 4.63 | 4.68 | 4.74 | 4.48 | 5.49 | 5.25 | 5.38 | 5.25 |
| Jarosite-K | − 3.09 | − 2.31 | − 1.82 | − 1.81 | − 2.94 | − 2.34 | − 3.39 | − 2.31 | − 1.9 | − 1.47 | − 2.42 | − 1.66 |
| K-feldspar | 2.39 | 2.01 | 3.11 | 2.49 | 2.04 | 2.03 | 2.11 | 1.89 | 2.71 | 2.51 | 2.72 | 2.54 |
| K-mica | 11.55 | 11.14 | 12.27 | 11.93 | 11.07 | 11.24 | 11.19 | 11 | 12 | 11.83 | 11.84 | 11.84 |
| Kaolinite | 5.98 | 5.7 | 6.22 | 6.16 | 5.7 | 5.79 | 5.78 | 5.66 | 6.15 | 6.04 | 6 | 6.03 |
| Manganite | − 6.79 | − 7.04 | − 5.42 | − 6.56 | − 7.19 | − 7.29 | − 7.24 | − 7.4 | − 6.53 | − 6.52 | − 6.32 | − 6.67 |

**Table 5** continued

| Sample name | Th-S1 | | Th-S2 | | Th-S3 | | Th-S4 | | Th-S5 | | Th-S6 | |
| --- | --- | --- | --- | --- | --- | --- | --- | --- | --- | --- | --- | --- |
| Date | January | April | January | April | January | April | January | April | January | April | January | April |
| Melanterite | − 6.94 | − 6.87 | − 6.98 | − 6.73 | − 6.86 | − 6.71 | − 7.05 | − 6.71 | − 6.74 | − 6.65 | − 7.01 | − 6.64 |
| $O_2(g)$ | − 38.04 | − 36.68 | − 38.68 | − 37.6 | − 37.29 | − 37.03 | − 37.01 | − 36.65 | − 37.72 | − 37.54 | − 37.81 | − 37.66 |
| Otavite | − 2.22 | − 2.69 | − 2.33 | − 2.57 | − 2.63 | − 2.91 | − 2.61 | − 3 | − 2.72 | − 2.79 | − 2.62 | − 2.76 |
| Pyrochlorite | − 7.67 | − 7.83 | − 6.76 | − 7.51 | − 7.94 | − 8 | − 7.97 | − 8.07 | − 7.49 | − 7.46 | − 7.35 | − 7.58 |
| Pyrolusite | − 11.3 | − 10.83 | − 10.65 | − 10.93 | − 11.23 | − 11.17 | − 11.13 | − 11.07 | − 10.97 | − 10.85 | − 10.86 | − 11.03 |
| Quartz | 0.78 | 0.66 | 0.9 | 0.73 | 0.71 | 0.66 | 0.72 | 0.64 | 0.8 | 0.73 | 0.81 | 0.74 |
| Rhodochrosite | − 1.14 | − 1.23 | − 0.79 | − 1.12 | − 1.22 | − 1.32 | − 1.22 | − 1.36 | − 0.96 | − 1.01 | − 0.9 | − 1.09 |
| Sepiolite | − 2.57 | − 2.95 | − 0.83 | − 2.4 | − 3.06 | − 3.32 | − 2.99 | − 3.46 | − 2.02 | − 2.43 | − 1.79 | − 2.54 |
| Sepiolite(d) | − 5.55 | − 6.06 | − 3.62 | − 5.4 | − 6.14 | − 6.44 | − 6.1 | − 6.61 | − 5.01 | − 5.43 | − 4.75 | − 5.54 |
| Siderite | − 1.56 | − 1.38 | − 1.36 | − 1.23 | − 1.49 | − 1.35 | − 1.62 | − 1.36 | − 1.2 | − 1.09 | − 1.37 | − 1.18 |
| $SiO_2(a)$ | − 0.44 | − 0.53 | − 0.37 | − 0.49 | − 0.49 | − 0.53 | − 0.46 | − 0.53 | − 0.42 | − 0.49 | − 0.42 | − 0.48 |
| Smithsonite | − 3.66 | − 4.31 | * | − 3.31 | − 0.78 | − 3.57 | * | − 4 | − 3.95 | * | − 4.13 | 3.5 |
| Strontianite | − 0.69 | − 0.82 | − 0.3 | − 0.66 | − 0.25 | − 0.88 | − 0.74 | − 0.92 | − 0.53 | − 0.61 | − 0.44 | − 0.64 |
| Talc | 0.2 | 0.03 | 2.25 | 0.51 | − 4.81 | − 0.54 | − 0.08 | − 0.62 | 1.01 | 0.49 | 1.27 | 0.32 |
| Willemite | − 5.95 | − 7.09 | * | − 4.98 | * | − 5.77 | * | − 6.6 | − 6.52 | * | − 6.79 | − 5.54 |
| Witherite | − 4.63 | − 4.68 | − 4.24 | − 4.52 | * | − 4.84 | − 4.7 | − 4.84 | − 4.58 | − 4.66 | − 4.5 | − 4.65 |
| $Zn(OH)_2(e)$ | − 5.38 | − 6.13 | * | − 4.89 | * | − 5.47 | * | − 5.96 | − 5.67 | * | − 5.76 | − 5.19 |

that fluorite has more solubility at higher temperature (Ellis and Mahon 1964; Majumdar et al. 2009).

At 60–90 °C all SIs approach zero and equilibrium state, so more evaluation with assessing the chemical geothermometers must be conducted to judge about the most probable temperature of the reservoir.

## Discussion

In the following sections processes and factors that control the chemistry of the studied thermal waters (mineral dissolution, dedolomitization and mixing) and heating mechanism (temperature and circulation depth of thermal waters) are discussed and a conceptual flow model for the thermal springs is suggested.

### Mineral dissolution

The Na/Cl ratios for the thermal springs were found to be around unity, which indicates the halite dissolution is the source of Na in the thermal springs (Fig. 12). Accumulations of Na and Cl in the crystal lattice of minerals in Lar Formation probably caused the increase in these two ions in the thermal waters. On the other hand, the leaching of the evaporite salts from the unsaturated zone due to the high evaporation rate in this area could cause the Na–Cl water type (Adams et al. 2001).

The high concentration of Ca and Mg and the value of calcite and dolomite saturation rate (usually higher than zero) in thermal waters are associated with the carbonate reservoir rock (Favara et al. 1998; Mohammadi et al. 2010). Mg/Ca molar ratios can be used to differentiate limestone and dolomite groundwater sources. The relationship between Ca, Mg and Na concentrations in all of the samples in both wet and dry seasons is presented in Fig. 13. Mg/Ca and Na/Ca molar ratios range from 0.46 to 0.77 and 10.24 to 15.16 in the thermal springs, respectively. Negative correlation between the Cl and Mg concentrations suggests a deep geothermal reservoir (Chulli et al. 2012; Ellis 1971). However, a positive relationship between Mg and Cl in more saline waters (Th-S5–6) with lower temperature and higher calcite and dolomite saturation indices (Fig. 6f and Table 4) can indicate that dolomite dissolved along the flow path from recharge to the discharge region.

Relatively high sulfate concentration in the thermal springs can be attributed to dissolution of the carbonate and sulfate cement. The association of sulfate with chloride concentration in two thermal springs (Th-S5–6) shows that the dissolution of evaporite minerals is the likely source of sulfate in thermal waters. Interaction with the minerals in the upper and lower stratum (Fajan and Shemshak Formations, respectively) and, to some extent, dissolution of other sulfate minerals such as celestite (Fig. 15) and barite probably caused an increase in sulfate concentration in the thermal waters (Ashjari and Raeisi 2006). The relationship of Co-S5 with the $SO_4$ corner in Fig. 7 reveals probable dissolution of gypsum from the gypsum lenses of the Fajan Formation.

According to the results of Ellis and Mahon (1964), near-neutral pH waters (6.5–8) and saturated on amorphous silica have more soluble fluoride content. In general, fluoride content in water is due to the dissolution of minerals such as fluorite, apatite, cryolite and hornblende especially in the semi-arid climate with alternative wet and dry conditions. Also, anion exchange process releases F which binds with OH (particularly at the alkaline groundwater) or Cl (Cabrera et al. 2001; Shaji et al. 2007). Besides, increasing concentration of F in the thermal carbonate

**Fig. 12** Relationship between the Na/Cl and EC in the sample analyzed in January and April
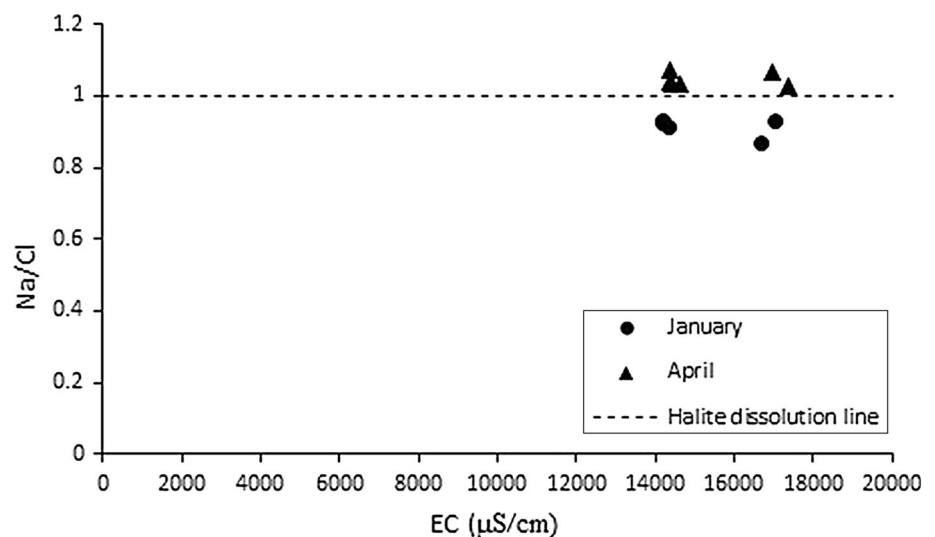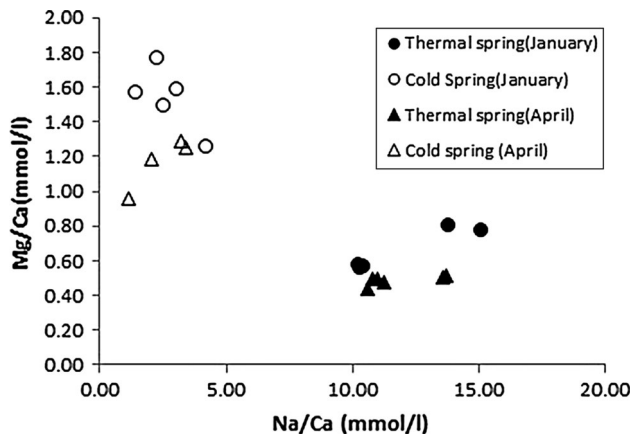
**Fig. 13** Relationship between Mg/Ca and Na/Ca in all analyzed samples in wet (January) and dry (April) seasons

groundwater can be related to the calcite precipitation that enhances the dissolution of fluorite (Ma et al. 2011).

The relationship between Sr/Ca ratios and Cl in all the samples analyzed in January and April is shown in Fig. 14. Sr/Ca ratio is higher in the thermal springs, and by increasing the concentration of Cl, it is enhanced. The reduction in Sr/Ca ratios indicates that carbonate dissolution/re-precipitation reaction controls the Sr enrichment, as an incompatible element (Gunn et al. 2006).

The plot of saturation index of celestite versus $SO_4$ concentrations in the thermal waters indicates a significant correlation ($r^2 = 0.85$) (Fig. 15). So, the elevated concentration of Sr in the thermal springs can be controlled by the dissolution of celestite impurity in the aquifer (Mustafa et al. 2015).

Figure 16 shows Li–Rb–Cs triangular diagram for the thermal waters in January 2015. Plotting of the thermal waters within the domain of rock dissolution suggests that these elements in the thermal waters were originated from
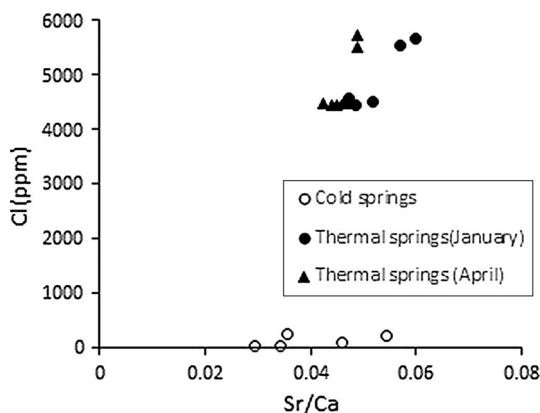


**Fig. 14** Relation between chloride versus Sr/Ca for thermal and cold waters analyzed in January and April

the reservoir rocks (Giggenbach 1991; Pasvanoglu and Chandrasekharam 2011; Shakeri et al. 2008).

### Dedolomitization

Semnan thermal springs are in equilibrium or supersaturated with calcite and dolomite and undersaturated with gypsum and halite (Table 5). Dissolution of gypsum or anhydrite causes the Ca concentration increases which the common ion effect could force precipitation of calcite and decrease the pH and $HCO_3$. Therefore, removal of carbonate ion promotes the dissolution of dolomite and increases the concentration of Mg and $CO_2$ gas (Fig. 17a, d). This process is called dedolomitization, and it has been widely documented for numerous aquifers (e.g., Back et al. 1983; Plummer et al. 1990; Ma et al. 2011; Lopez-Chicano et al. 2001; Moore et al. 2009).

The enrichment in $CO_2$ partial pressure between the recharge zone toward the down-gradient zone shows a closed system dominated in the aquifer (Back et al. 1983). A decrease in $HCO_3$ did not occur along with increasing $SO_4$ concentration (Fig. 17d). It seems that another hydrogeochemical reaction caused this enrichment (Plummer et al. 1990). The microbial sulfate reduction, which is represented by $H_2S$ odor, is probably responsible for additional $CO_2$ production (Machel et al. 1995). This behavior is consistent with the results of many case studies (e.g., Lopez-Chicano et al. 2001; Mohammadi et al. 2010; Marques et al. 2013).

### Mixing

A distinct positive correlation ($r^2 > 0.8$) between Cl and other elements indicates extensive dissolution of minerals from shallow to deep water circulation and accordingly longer resident time. Alçiçek et al. (2016) and Shakeri et al. (2008) attributed this positive correlation to the dilution of thermal water by shallow (i.e., cold) groundwater. Despite having a different temperature, the thermal springs have similar Cl values, especially in Th-S1–Th-S4 (Fig. 6a). Plotting the temperatures versus $SiO_2$ concentrations reveals that all water samples have a relatively similar $SiO_2$ concentration (Fig. 18). Temperature reduction without loss of $SiO_2$ content suggests that the conductive cooling during the ascending movement of water has occurred (Majumdar et al. 2009). So the difference between temperatures of the thermal spring may be caused by the differential conductive cooling and different groundwater flow paths.

However, an increase in the sodium–chloride ratio in April to more than one (Fig. 12) shows that an increase in Na or reduction in Cl has occurred. Cation exchange processes could explain the higher Na–Cl mole ratios in the dry season (April). But, as it can be seen in the plot of

Fig. 15 Hydrogeochemical relation between SI celestite and $SO_4$ in the thermal waters
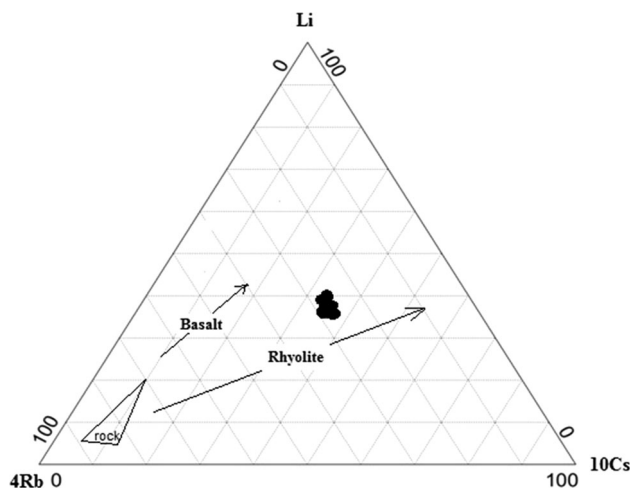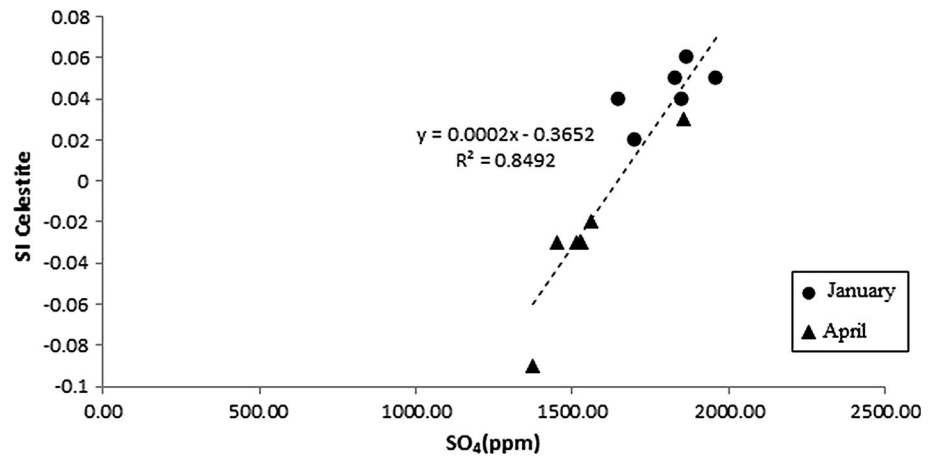


Fig. 16 Relative Li–Rb–Cs content in thermal waters collected in January 2015

Ca + Mg versus the $SO_4 + 0.5HCO_3$ unexpectedly Ca + Mg concentration does not change in thermal waters (Fig. 19). The thermal waters from different seasons plot near the dedolomitization trend line with a slope of 1 (Eberts and George 2000). No significant change in the concentration of elements in different seasons indicates that the chemical characteristics of thermal springs are affected by aquifer properties.

Low saturation indices with respect to carbonate minerals (Table 5) and low concentration of $SO_4$ in the dry season (Fig. 17) indicate that probably ascending thermal water mixed with fresh water is likely associated with previous precipitation events in wet (winter) season (Pasvanoğlu and Chandrasekharam 2011) and slow process of dilution in the phreatic storage waters. The slightly increasing Na/Cl ratio in the dry season is consistent with mixing with low chloride waters at shallow levels (Fig. 12). Similar results were reported by Uliana and Sharp (2001) who observed that during the large storm events because of the interaction between the low TDS

local recharge and saline waters from a regional flow system, calcite saturation index decreased and, as a consequence, the calcite dissolution occurs.

### Heating mechanism

#### Temperature of the thermal reservoir

The results of geothermometry (Table 4) show that different methods suggest different temperatures for the geothermal reservoir. One reason is possibly related to errors in the regression coefficient of the geothermometric equation (Du et al. 2005; Verma and Santoyo 1997; reported by Chandrajith et al. 2013), and another one is that the applicability of a geothermometer is dependent on a series of assumptions. Chemical equilibrium at depth without re-equilibration upon cooling and boiling and non-mixing of the thermal water with cold surface waters in upward flow zones is the most important one (Arnorsson 1983).

Figure 10 shows that the evolution trend from the cold water toward the thermal waters is recognizable and represents the water–rock interaction in the reservoir. Therefore, application of cation geothermometers is potentially erroneous because the mineral assemblage of carbonate rocks probably controls the water chemistry (Marini et al. 1986).

The silica-based geothermometers are widely used to calculate the temperature of low enthalpy reservoir (Back et al. 1983; Mohammadi et al. 2010) because $SiO_2$ is not influenced by the formation of complexes, common ion effect and loss of volatile components at low temperatures (Fournier 1977). There are no specific rules for selecting the silica form as a correct geothermometer for estimating the reservoir temperature. According to Fournier (1979) and Kharaka et al. (1977) quartz geothermometer is more suitable for a higher reservoir temperature ($> 150$ and $> 70\ °C$, respectively), while for one with a lower
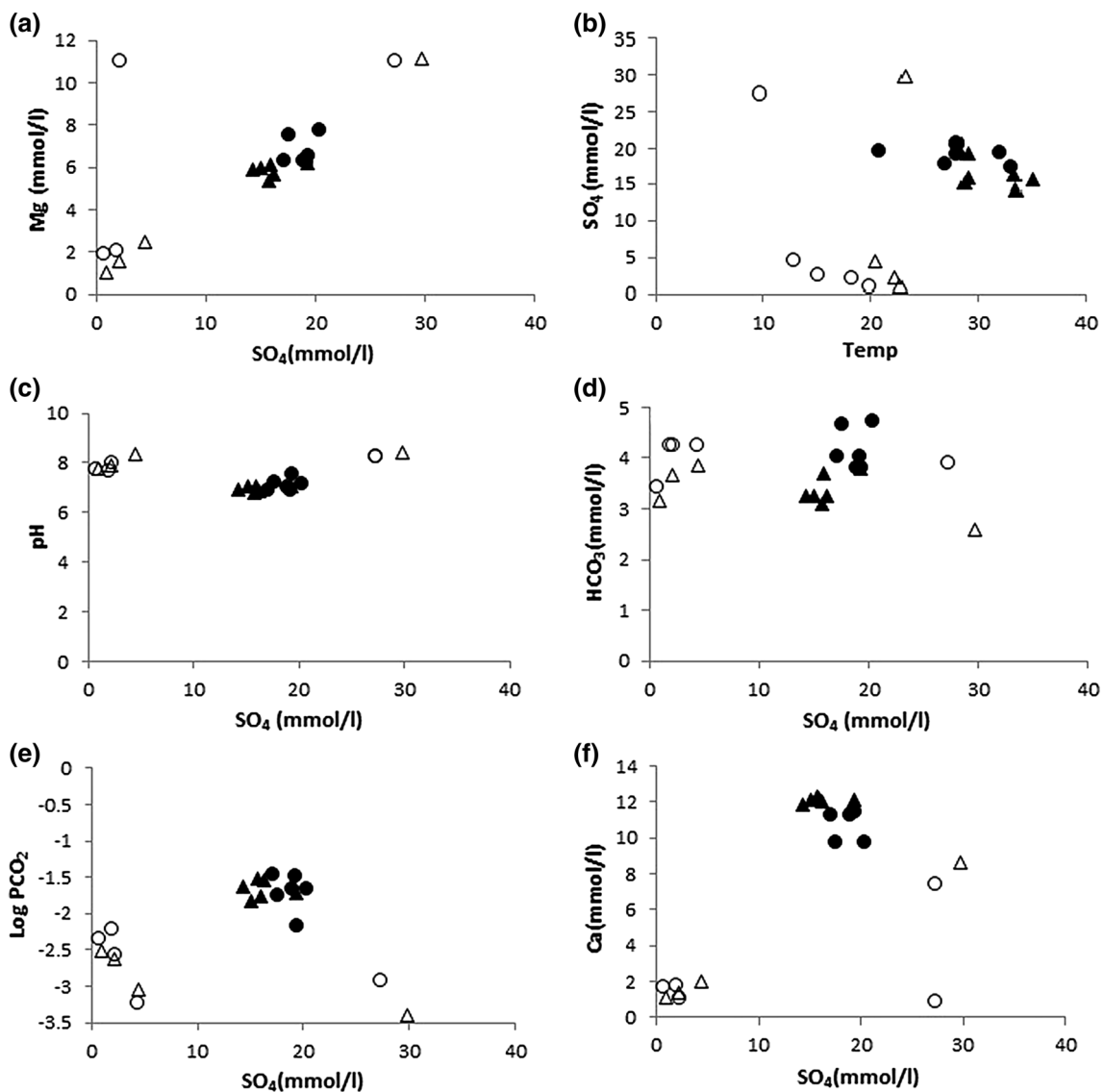
**Fig. 17** Relationship between the temperature, $HCO_3$, Ca, Mg, pH, $PCO_2$ and $SO_4$ content. Symbols are as in Fig. 13

temperature application of chalcedony geothermometer is reliable.

Because of partial equilibrium condition the K–Mg, quartz and chalcedony geothermometers (Fig. 9 and Table 4) are more reliable particularly if we take into account the results of saturation index calculations (Fig. 11). It seems that the average temperature of the reservoir is in the range of 60–80 °C. Due to the dilution effect by precipitation in April, the estimated temperature is just a few degrees lower than the January temperature.

*Circulation depth of the thermal water*

The results of the physical and hydrogeochemical data set of the cold and thermal waters made it possible to suggest a conceptual circulation model for the thermal springs. The

conceptual circulation model could provide valuable insight into the environmental processes controlling recharge and chemistry of the thermal waters. Higher mineralization as well as the higher temperature of the thermal waters in comparison with the cold waters reflects a deep circulation for groundwater. Deep groundwater originated from infiltration of meteoric water through the dolomitized carbonate outcrop in the Chenaran Mountain (Fig. 20). The Chenaran Mountain was uplifted by the action of a reverse fault that rises up the limestone and dolomitized Lar Formation to the surface at an elevation of 2400 m AMSL. The hydraulic connection between the northern and southern flanks is restricted to the southwestern plunge, since the elevation of the impermeable Shemshak Formation under the anticline ridge is high, as shown in Fig. 4. The Anzab fault is at the foot of the
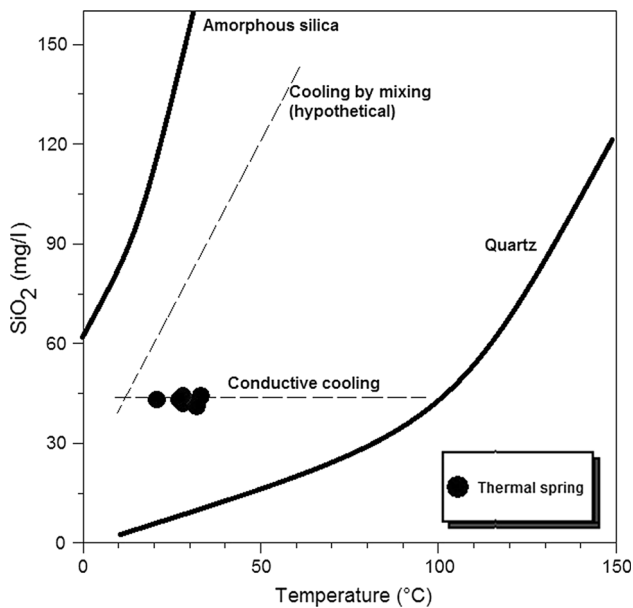
**Fig. 18** Plot of $SiO_2$ content versus temperature. The solid lines represent the quartz and amorphous silica solubility, and broken lines are hypothetical trend for mixing and conductive cooling
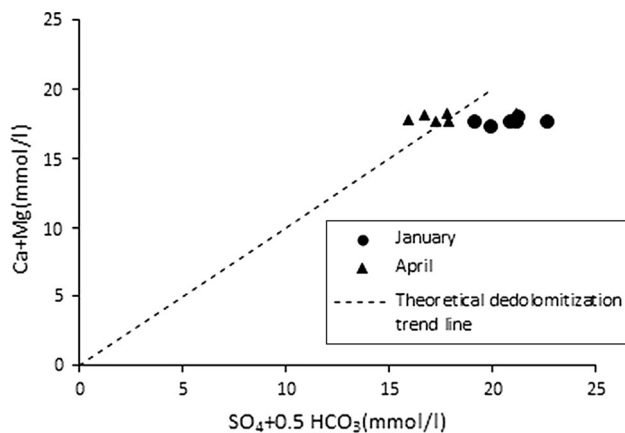


**Fig. 19** Concentration of Ca + Mg as a function of concentration of $SO_4$ + 0.5$HCO_3$ in thermal waters in two dry and wet seasons

Chenaran Anticline and parallel to the strike. This normal fault shifts down the carbonate formation and causes probable hydrogeological disconnection between this anticline and the adjacent syncline. In this circumstance, the karst water probably flows parallel to the strike, at the foot of anticline toward the southwestern plunge, and then flows to the adjacent syncline. As a result, the karst water in the form of the thermal waters discharges from springs located close to a locally oriented NE–SW reverse fault and dips toward the south. This fault puts the shale and sandstone rocks from the Lower Jurassic (Shemshak Formation, Js-s in Fig. 4) in contact with the karstic formation from the Upper Jurassic (Jl-2) in the eastern trail. The karst water should have the $HCO_3$-type water. However, high Cl

and $SO_4$ anions disrupt our expectation. The thermal springs emerge through the above-mentioned fault (Fig. 20) from the dolomitic Lar Formation which is sandwiched between the Shemshak and Fajan Formations. As the result of water–rock interactions, the lithology of these formations could elevate the ion concentration of the thermal waters (Ashjari and Raeisi 2006).

## Conclusion

The physicochemical characteristics of Semnan thermal springs and five cold springs in their vicinity area were evaluated in two wet and dry seasons. Water samples were classified according to temperature, pH, TDS and major ion contents as cold and thermal springs. Cold springs are mainly mixed cation with $HCO_3$ and $SO_4$ types with temperature from 9.8 to 23 °C, TDS from 346 to 3060 mg/l and pH from 7 to 8.23, while thermal springs are mainly Na–Cl and Na–Cl–$SO_4$ types with temperature from 20.9 to 35.1 °C, TDS from 9460 to 11,580 mg/l and pH from 6.81 to 7.48.

A lower concentration of F, Si, Sr, Li and some trace elements and major ion content in the cold spring waters show that they flow in shallow depths and experience lower water–rock interaction, while thermal springs circulated from deeper levels, where they could reach a higher temperature. There is no significant temporal change in the concentration of elements, representing a mechanism of diffuse flow in the aquifer. The twofold increase in some ions such as iron, chromium and nickel in the dry season is attributed to the reduction in pH and higher temperature in April or the dilution effect of precipitation in January. The results reveal that carbonate dissolution/re-precipitation reaction and dissolution of celestite and fluorite control the Sr and F enrichment, respectively.

The thermal springs with different temperatures have similar chemical characteristics. Variation is mostly attributed to different conductive cooling of thermal waters. The chemical composition of thermal waters is controlled by dolomite, halite and sulfate minerals dissolution, bacterial sulfate reduction and calcite precipitation under a closed condition with respect to $CO_2$, and it is modified by calcite dissolution by dilution effect caused by the heavy rainfall. Dedolomitization process and water–rock interaction with the confining sandstone formation can enhance the concentrations of some ions such as K and $SiO_2$.

All thermal spring waters fall into the field of partially equilibrated waters in Na–K–Mg ternary diagram of Giggenbach. The K–Mg (in Giggenbach diagram), quartz and chalcedony geothermometers provide a more reliable subsurface temperature for the investigated waters than
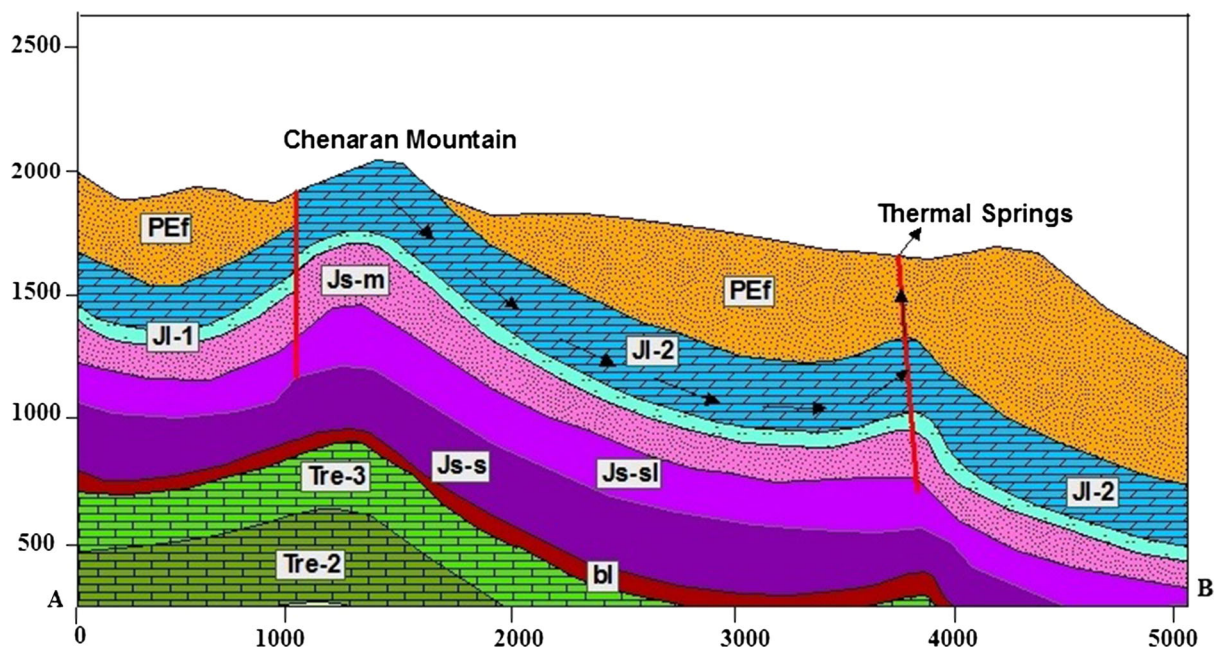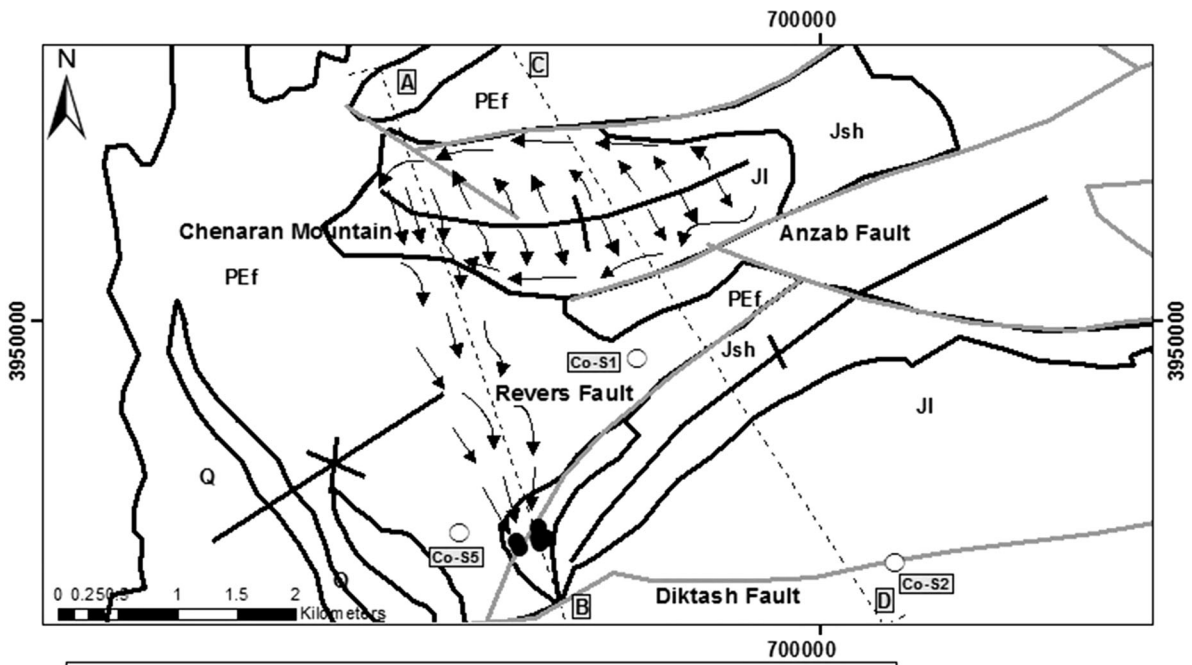
◀**Fig. 20** Proposed model for groundwater flow of the thermal springs in the study area

Na–K, Na–K–Ca, Mg–Li and Na–Li geothermometers. The estimated average temperature of the reservoir is in the range of 60–80 °C, which possibly occurs at a depth of about 2–2.5 km from the surface. These temperature estimates are in the same range as the ones obtained using the saturation index method.

Based on all the information obtained in this work, it seems that an increase in water temperature is mainly due to a depth circulation of meteoric water at calcareous dolomitic rocks. The infiltrated water flows from the Chenaran karstic anticline toward the adjacent syncline, and heated water moved up to the surface through the major faults that interrupt the layering and cut the impermeable cap rock. The maintenance of water chemical qualities such as TDS and temperature values during the storm flow and little change in the concentration of ions provide evidence that these springs are suitable for expanding spa facilities. Since the studied thermal springs recharge Abgarm River in the Semnan plain, the Semnan aquifer is at the risk of getting polluted by the salt water intrusion. Therefore, this study helps manage the quality of groundwater in the Semnan plain.

# References

Adams S, Titus R, Pietersen K, Tredoux G, Harris C (2001) Hydrochemical characteristics of aquifers near Sutherland in the Western Karoo, South Africa. J Hydrol 241(1):91–103

Alavi M (1991) Sedimentary and structural characteristics of the Paleo-Tethys remnants in northeastern Iran. Geol Soc Am Bull 103:983–992

Alavi M (2004) Regional stratigraphy of the Zagros fold-thrust belt of Iran and its pro-foreland evolution. Am J Sci 304:1–20

Alçiçek H, Bülbül A, Alçiçek MC (2016) Hydrogeochemistry of the thermal waters from the Yenice geothermal field (Denizli Basin, Southwestern Anatolia, Turkey). J Volcanol Geotherm Res 309:118–138

Arnorsson S (1983) Chemical equilibria in Icelandic geothermal systems—implications for chemical geothermometry investigations. Geothermics 12(2):119–128

Arnorsson S, Gunnlaugsson E, Svavarsson H (1983) The chemistry of geothermal waters in Iceland. III. Chemical geothermometry in geothermal investigations. Geochim Cosmochim Acta 47:567–577

Ashjari J, Raeisi E (2006) Lithological control on water chemistry in karst aquifers of the Zagros Range, Iran. Cave Karst Sci 33(3):111

Asta MP, Gimeno MJ, Auqué LF, Gómez J, Acero P, Lapuente P (2012) Hydrochemistry and geothermometrical modeling of low-temperature Panticosa geothermal system (Spain). J Volcanol Geotherm Res 235:84–95

Back W, Hanshaw BB, Plummer LN, Rahn PH, Rightmire CT, Rubin M (1983) Process and rate of dedolomitization: mass transfer and 14C dating in a regional carbonate aquifer. Geol Soc Am Bull 94(12):1415–1429

Ben Brahim F, Makni J, Bouri S, Ben Dhia H (2014) Evaluation of temperature and mixing process of water in deep and shallow aquifers in the Southwestern Tunisia: case of Djerid Region. Arab J Sci Eng 39(7):5677–5689

Cabrera A, Blarasin M, Villalba G (2001) Groundwater contaminated with arsenic and fluoride in the Argentine Pampean plain. J Environ Hydrol 9(6):1–9

Calmbach L (1997) AquaChem computer code-version 3.7.42. Waterloo Hydrogeologic, Waterloo

Chandrajith R, Barth JA, Subasinghe ND, Merten D, Dissanayake CB (2013) Geochemical and isotope characterization of geothermal spring waters in Sri Lanka: evidence for steeper than expected geothermal gradients. J Hydrol 476:360–369

Chebotarev II (1955) Metamorphism of natural waters in the crust of weathering. Geochim Cosmochim Acta 8, part 1:22–48, part 2:137–170, part 3:198–212

Chulli B, Davraz A, Makni J, Bedir M, Ben Dhia H (2012) Hydrogeological investigation of thermal waters in the Sfax Basin (Tunisia). Environ Earth Sci 66:1–16

D'Amore F, Fancelli R, Caboi R (1987) Observation on the application of chemical geothermometers to some hydrothermal systems in Sardinia. Geothermics 16:271–282

Darvishzade A (1991) Geology of Iran. Sepehr Publication, Tehran **(in Persian)**

Du J, Liu C, Fu B, Ninomiya Y, Zhang Y, Wang C, Wang H, Sun Z (2005) Variations of geothermometry and chemical-isotopic compositions of hot spring fluids in the Rehai geothermal field, southwestern China. J Volcanol Geotherm Res 142(3):243–261

Eberts SM, George LL (2000) Regional ground-water flow and geochemistry in the Midwestern Basins and Arches aquifer system in parts of Indiana, Ohio, Michigan, and Illinois: by Sandra M. Eberts and Lori L. George (No. 1423). US Geological Survey

Ellis AJ (1971) Magnesium ion concentrations in the presence of Mg-chlorite, calcite, carbon dioxide, and quartz. Am J Sci 271:481–489

Ellis AJ, Mahon WAJ (1964) Natural hydrothermal systems and experimental hot water/rock interactions. Geochim Cosmochim Acta 28:1323–1357

Farr G, Bottrell S (2013) The hydrogeology and hydrochemistry of the thermal waters at Taffs Well, South Wales, UK. Cave Karst Sci Trans Br Cave Res Assoc 40(1):5–12

Favara R, Grassa F, Inguaggiato S (1998) Geochemical and hydrogeological characterization of thermal springs in Western Sicily, Italy. J Volcanol Geotherm Res 84(1):125–141

Fouillac C, Michard G (1981) Sodium/lithium ratio in water applied to geothermometry of geothermal reservoirs. Geothermics 10(1):55–70

Fournier RO (1977) Chemical geothermometers and mixing models for geothermal systems. Geothermics 5:41–50

Fournier RO (1979) Geochemical and hydrologic considerations and the use of enthalpy-chloride diagrams in the prediction of underground conditions in hot spring system. J Volcanol Geotherm Res 5:1–16

Fournier RO, Truesdell AH (1973) An empirical Na–K–Ca geothermometer for natural waters. Geochim Cosmochim Acta 37:1255–1275

Ghafori M (1987) Recognition of Iran mineral water and springs. Tehran University Publication, Tehran **(in Persian)**

Giggenbach WF (1988) Geothermal solute equilibria. Derivation of Na–K–Mg–Ca geoindicators. Geochim Cosmochim Acta 52:2749–2765

Giggenbach WF (1991) Chemical techniques in geothermal exploration. In: D'Amore F (ed) Application of geochemistry in geothermal reservoir development. UNITAR/UNDP Centre on Small Energy Resources, Rome, pp 119–144

Giggenbach W, Glover RB (1992) Tectonic regime and major processes governing the chemistry of water and gas discharges from the Rotorua geothermal field, New Zealand. Geothermics 21:121–140

Gokgoz A, Tarcan G (2006) Mineral equilibria and geothermometry of the Dalaman–Kovcegiz thermal springs, southern Turkey. Appl Geochem 21:253–268

Gunn J, Bottrell SH, Lowe DJ, Worthington SR (2006) Deep groundwater flow and geochemical processes in limestone aquifers: evidence from thermal waters in Derbyshire, England, UK. Hydrogeol J 14(6):868–881

Han DM, Liang X, Jin MG, Currell MJ, Song XF, Liu CM (2010) Evaluation of groundwater hydrochemical characteristics and mixing behavior in the Daying and Qicun geothermal systems, Xinzhou Basin. J Volcanol Geotherm Res 189(1):92–104

Kabata-Pendias A, Mukherjee AB (2007) Trace elements from soil to human. Springer, New York

Karimi H, Moore F (2008) The source and heating mechanism for the Ahram, Mirahmad and Garu thermal springs, Zagros Mountains, Iran. Geothermics 37(1):84–100

Karingithi CW (2009) Chemical geothermometers for geothermal exploration. Presented at short course IV on exploration for geothermal resources, organized by UNU-GTP, KenGen and GDC, Lake Naivasha, Kenya

Kharaka YK, Mariner RH (1989) Chemical geothermometers and their application to formation waters from sedimentary basins. In: Näser ND, McCulloh TH (eds) Thermal history of sedimentary basins; methods and case histories. Springer, New York, pp 99–117

Kharaka YK, Callender E, Carothers WW (1977) Geochemistry of geopressured geothermal waters from the Texas Gulf Coast (No. CONF-771153-P1-7)

Kompani-Zare M, Moore F (2001) Chemical thermometry and origin of the Dalaki mineral springs, Bushehr Province, Iran. J Hydrol 40(2):189–204

Lambrakis N, Kallergis G (2005) Contribution to the study of Greek thermal springs: hydrogeological and hydrochemical characteristics and origin of thermal waters. Hydrogeol J 13(3):506–521

Langmuir D (1997) Aqueous environmental geochemistry, vol 549. Prentice Hall, Upper Saddle River

Lopez-Chicano M, Bouamama M, Vallejos A, Pulido-Bosch A (2001) Factors which determine the hydrogeochemical behaviour of karstic springs. A case study from the Betic Cordilleras, Spain. Appl Geochem 16(9):1179–1192

Ma T, Wang Y, Guo Q, Yan C, Ma R, Huang Z (2009) Hydrochemical and isotopic evidence of origin of thermal karst water at Taiyuan, northern China. J Earth Sci 20(5):879–889

Ma R, Wang Y, Sun Z, Zheng C, Ma T, Prommer H (2011) Geochemical evolution of groundwater in carbonate aquifers in Taiyuan, northern China. Appl Geochem 26(5):884–897

Machel HG, Krouse HR, Sassen R (1995) Products and distinguishing criteria of bacterial and thermochemical sulfate reduction. Appl Geochem 10(4):373–389

Majumdar N, Mukherjee AL, Majumdar RK (2009) Mixing hydrology and chemical equilibra in Bakreswar geothermal area, Eastern India. J Volcanol Geotherm Res 183:201–212

Marini L, Chiodini G, Cioni R (1986) New geothermometers for carbonate—evaporite geothermal reservoirs. Geothermics 15(1):77–86

Marques JM, Graça H, Eggenkamp HG, Neves O, Carreira PM, Matias MJ, Mayer B, Nunes D, Trancoso VN (2013) Isotopic and hydrochemical data as indicators of recharge areas, flow paths and water–rock interaction in the Caldas da Rainha–Quinta das Janelas thermomineral carbonate rock aquifer (Central Portugal). J Hydrol 476:302–313

Mohammadi Z, Parizi HS (2013) Hydrogeochemistry and geothermometry of the Jowshan thermal spring, central Iran. Geochem Int 51(12):994–1004

Mohammadi Z, Bagheri R, Jahanshahi R (2010) Hydrogeochemistry and geothermometry of Changal thermal springs, Zagros region, Iran. Geothermics 39(3):242–249

Moore PJ, Martin JB, Screaton EJ (2009) Geochemical and statistical evidence of recharge, mixing, and controls on spring discharge in an eogenetic karst aquifer. J Hydrol 376(3):443–455

Mustafa O, Merkel B, Weise SM (2015) Assessment of hydrogeochemistry and environmental isotopes in karst springs of Makook Anticline, Kurdistan Region, Iraq. Hydrology 2(2):48–68

Nabavi MH (1976) An introduction to the geology of Iran. Geological Survey of Iran, Tehran (in Persian)

Nabavi MH (1987) Geological map of Iran, 1:100,000 series sheet 6661, Semnan. Geological Survey of Iran, Tehran (with explanation in Persian)

Nicholson K (1993) Geothermal fluids, chemistry and exploration techniques. Springer, Berlin

Noorollahi Y, Yousefi H, Itoi R, Ehara S (2009) Geothermal energy resources and development in Iran. Renew Sustain Energy Rev 13:1127–1132

Parkhurst DL, Appelo CAJ (1999) User's guide to PHREEQC (version 2): a computer program for speciation, batch reaction, one dimensional transport and inverse geochemical calculations. Water resources investigations, report 9524259, US Geological Survey, Denver, Colorado

Pasvanoğlu S, Chandrasekharam D (2011) Hydrogeochemical and isotopic study of thermal and mineralized waters from the Nevşehir (Kozakli) area, Central Turkey. J Volcanol Geotherm Res 202(3):241–250

Plummer LN, Busby JF, Lee RW, Hanshaw BB (1990) Geochemical modeling of the Madison aquifer in parts of Montana, Wyoming, and South Dakota. Water Resour Res 26(9):1981–2014

Pürschel M, Gloaguen R, Stadler S (2013) Geothermal activities in the Main Ethiopian Rift: hydrogeochemical characterization of geothermal waters and geothermometry applications (Dofan-Fantale, Gergede-Sodere, Aluto-Langano). Geothermics 47:1–12

Raghimi M, Yakhkashi ME (2002) The origin of thermal water of Ziarat, Gorgan by hydrochemistry and isotopic studies. J Agric Sci Nat Resour 9(3):29–40 (in Persian, with abstract in English)

Reed M, Spycher N (1984) Calculation of pH and mineral equilibria in hydrothermal waters with application to geothermometry and studies of boiling and dilution. Geochim Cosmochim Acta 48:1479–1492

Shahidi A, Barrier E, Brunet MF, Saidi A (2008) Tectonic evolution and Late Triassic-Middle Eocene extension in central Alborz, Iran. Geoscience 17(1):4–25

Shaji E, Bindu JV, Thambi DS (2007) High fluoride in groundwater of Palghat District, Kerala. Curr Sci 92(2):240

Shakeri A, Moor F, Kompani-Zare M (2008) Geochemistry of the thermal springs of Mount Taftan, southeastern Iran. J Volcanol Geotherm Res 178:829–836

Shamsi A, Kazemi G (2014) A review of research dealing with isotope hydrology in Iran and the first Iranian meteoric water line. Geopersia 4(1):73–86

Sharifi R, Moore F, Mohammadi Z, Keshavarzi B (2016) Estimation of deep water temperature and hydrogeochemistry of springs in

the takab geothermal field, West Azarbaijan, Iran. Environ Monit Assess 188:75

Stöcklin J (1968) Structural history and tectonics of Iran. A review. AAPG Bull 52(7):1229–1258

Stöcklin J, Setudehnia A (1991) Stratigraphic lexicon of Iran. Geol Surv Iran Rep 18(3'd edition):1–376

Szczucińska AM, Siepak M, Zioła-Frankowska A, Marciniak M (2010) Seasonal and spatial changes of metal concentrations in groundwater outflows from porous sediments in the Gryżyna-Grabin Tunnel Valley in western Poland. Environ Earth Sci 61(5):921–930

Tarcan G, Gemici U (2003) Water geochemistry of the Seferihisar geothermal area, İzmir, Turkey. J Volcanol Geochem Res 126:225–242

Uliana MM, Sharp JM (2001) Tracing regional flow paths to major springs in Trans-Pecos Texas using geochemical data and geochemical models. Chem Geol 179(1–4):53–72

Verma SP, Santoyo E (1997) New improved equations for Na/K, Na/Li and $SiO_2$ geothermometers by outlier detection and rejection. J Volcanol Geotherm Res 79(1–2):9–23

Yazdi M, Taheri M, Navi P (2015) Environmental geochemistry and sources of natural arsenic in the Kharaqan hot springs, Qazvin, Iran. Environ Earth Sci 73(9):5395–5404

Yousefi H, Ehara S, Noorollahi Y (2007) Geothermal potential site selection using GIS in Iran. In: Proceeding of the 32nd workshop on geothermal reservoir engineering, pp 174–182

Yousefi H, Noorollahi Y, Ehara S, Itoi R, Yousefi A, Fujimitsu Y, Nishijima J, Sasaki K (2010) Developing the geothermal resources map of Iran. Geothermics 39(2):140–151

Zhang X, Guo Q, Li J, Liu M, Wang Y, Yang Y (2015) Estimation of reservoir temperature using silica and cationic solutes geothermometers: a case study in the Tengchong geothermal area. Chin J Geochem 34(2):233–240

Zheng XL, Liu HJ (1996) Let us compare the above. J Xi'an Coll Geol 18(1):74–79